Modeling vascular disease using self-assembling human induced pluripotent stem cell derivatives in 3D vessels-on-chip

Nahon, D.M.

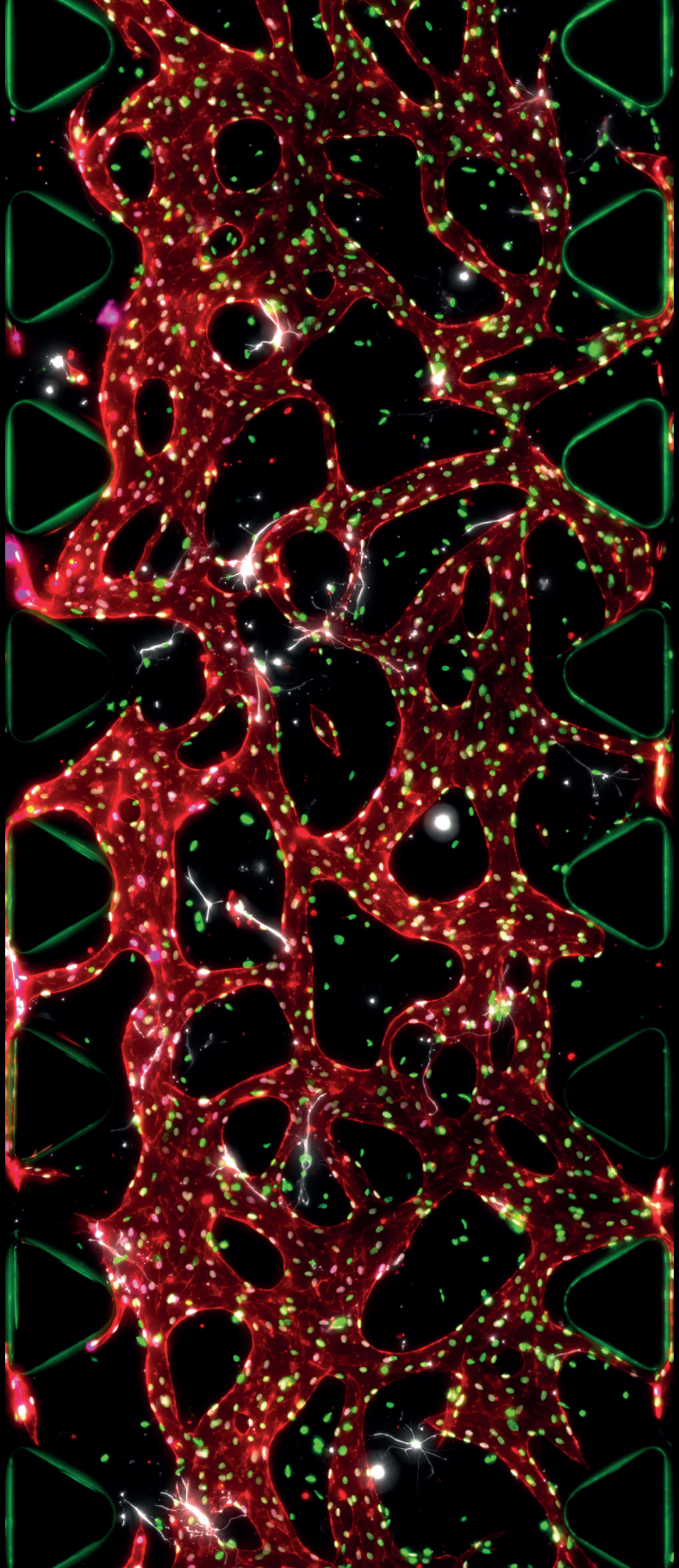

Chapter 2

Taking microphysiological systems to the next level: Why quantification of physiological features is essential

Abstract

Microphysiological systems (MPS) are cellular models that replicate aspects of organ and tissue function in vitro which can be used either individually or linked to each other. They are distinct from conventional cell cultures in that they include features such as gas- and fluid flow; for this reason, some are referred to as microfluidic Organs-on-Chip (OoCs). These advanced models can provide mechanical cues to cells as in real tissues, creating systems with the potential to impact understanding of human physiology and disease, toxic effects of the environment or drugs and the identification of novel therapeutics. To fulfill this potential, however, it is crucial to develop measurable standards that allow quantitative comparisons of MPS outcomes with physiological observations in humans so that their in vivo relevance and predictive value can be properly assessed as fit-for-purpose in specific applications. In this review we use MPS of the vascular system, intestine, brain and heart to illustrate the importance of quantifying physiological features of in vitro models for comparison with human in vivo observations and measuring variability between systems and operators. Specifically, we distinguish the quantification of 'designed features' that can be controlled in MPS design from 'emergent features' that describe cellular function within the device. We propose methods for improving MPS with read-outs and sensors that monitor complex physiology quantitatively and could lead to wider end-user adoption and regulatory acceptance.

This chapter is adapted from:
Standardizing designed and emergent quantitative features in microphysiological systems. Nature Biomedical Engineering. (2024) In press

Dennis M. Nahon, Renée Moerkens*, Hande Aydogmus, Bas Lendemeijer, Jeroen M. Stein, Adriana Martinez-Silgado, Milica Dostanić, Jean-Philippe Frimat, Cristina Gontan, Mees N.S. de Graaf, Michel Hu, Dhanesh G. Kasi, Lena S. Koch, Kieu T.T. Le, Sangho Lim, Heleen H.T. Middelkamp, Joram Mooiweer, Paul Motreuil-Ragot, Eva Niggl, Cayetano Pleguezuelos-Manzano, Jens Puschhof, Nele Revyn, José M. Rivera-Arbelaez, Jelle Slager, Laura M. Windt, Mariia Zakharova, Berend J. van Meer, Valeria V. Orlova, Femke M.S. de Vrij, Sebo Withoff, Massimo Mastrangeli, Andries van der Meer, and Christine L. Mummery*

Introduction

Microphysiological systems (MPS) are cellular models that recapitulate aspects of (human) physiology by recreating the dynamic microenvironment to which cells are exposed in organs or tissues. They often integrate features such as gas- and fluid flow and are then referred to as microfluidic Organs-on-Chip (OoCs). Their design may also allow incorporation of mechanical stimulation (e.g. contraction, stretch and strain) into living tissue constructs. Many MPS harbor multiple compartments that enable local microenvironments to be regulated independently to support different cell types, while still allowing communication between adjacent compartments. This facilitates complex co-culture in a single system or coupling of multiple MPS to model multi-organ interactions. The first examples of how these advanced model systems can impact toxicological, pharmaceutical and biomedical science are now beginning to emerge[1,2].

With increasing interest in using MPS, there is a pressing need to develop measurable standards to compare different systems and assess their *in vivo* relevance and predictive value. For this, it is essential to quantify physiological features of tissues in MPS and compare these with actual human (or animal) physiology *in vivo*. However, whilst MPS allow strict control over the culture microenvironment and are thus well-suited to quantify physiological features, most studies to date have only described their qualitative features. Realizing a shift towards quantitative outputs will require control over features such as compartment dimensions, fluid flow rates and system oxygen concentrations, as well as precision monitoring of cellular function (e.g. barrier integrity, electrophysiological properties, metabolite production, immune cell recruitment) inside the system. This will aid the development of measurable standards to qualify systems as fit-for-purpose i.e. suitable for measuring the parameter of interest, and will improve reproducibility of models between users. Qualification and standardization will take MPS technology to 'the next level' and ensure MPS become accepted options for regulatory agencies and end-users[3].

In this review, we (1) define and categorize quantifiable physiological features (2) provide an overview of physiological features of the human vascular system, intestine, heart and brain that are quantified in design or as read-outs of MPS (3) demonstrate how this approach enables the comparison between MPS and human *in vivo* observations and, finally (4) identify some key technical advances which could improve quantification of physiological features in MPS in the future.

Defining quantifiable physiological features for microphysiological systems

In essence, MPS use reverse-engineering to mimic specific organ- or tissue functions by incorporating and emulating essential cellular and biophysical components[4,5]. These are based on current understanding of human physiology: we define these as 'physiological features' in this review. In the context of quantitative modeling, it is helpful to categorize these features into 'designed' or 'emergent' (*Figure 1*). Importantly, features are not limited

to one of the two groups but can belong to both depending on the model and functional read-out required.

Designed features are physiological features directly translatable into device design or chemical or mechanical input. Examples include compartment dimensions, fluid flow dynamics and oxygen concentration. Designed features can be tightly regulated in MPS and are intended to be close mimics of *in vivo* conditions. Whether or not they are actually in a physiologically relevant range often depends on technical limitations in engineering and fabricating the device set-up.

Emergent features are physiological features that describe cellular function. These features cannot be completely controlled 'upfront' by device design or input; rather they develop in MPS as a result of intrinsic cellular properties and the microenvironment in the culture system. Examples of emergent features are barrier integrity of a cell layer, electrophysiological properties of the tissues or immune cell migration. Specialized sensors or downstream read-outs are required to monitor emergent features in MPS.

Quantifying emergent features in MPS can indicate physiological relevance and whether the particular device design is suitable for the intended application. Quantification of designed features provides insight into how design choice impacts emergent features and physiological output. In addition, quantitative control of designed features enhances the robustness of MPS and their reproducibility between users. Quantifying both designed and emergent features is essential if they are to be used, directly or indirectly, in developing measurable standards of physiological output in MPS. The selection of features relevant to integrate or monitor in any MPS depends on the specific research question. In general, 'as simple as possible, but as complex as necessary' is the guiding principle. This is in line with the widely accepted notion that MPS should be "fit-for-purpose" i.e. capture just one or a few features rather than having one complex device that serves all conceivable functions or applications[6]. This means that the designed features incorporated in an MPS should be limited to those necessary to induce the cellular organization and differentiation state required for physiologically relevant levels of the emergent features being investigated. Similarly, the sensors or read-outs should be limited to those sufficient for monitoring the emergent features of interest. Several causal relationships between designed and emergent features are well-established (e.g. oxygen concentration in an intestinal model impacts microbiome diversity). However, more often the exact implications of designed features have yet to be investigated. Quantification of both types of features in MPS will be necessary to reveal these interactions and provide insight into which designed features are required to create useful models for each goal.

The physiological relevance of any MPS depends on whether the quantified features actually reflect human physiological parameters. *In vitro* to *in vivo* translation requires critical evaluation of what kinds of data can be collected, how it is measured and normalized and which units might be used. We discuss this for the vascular system, intestine, heart and

brain in the sections below.

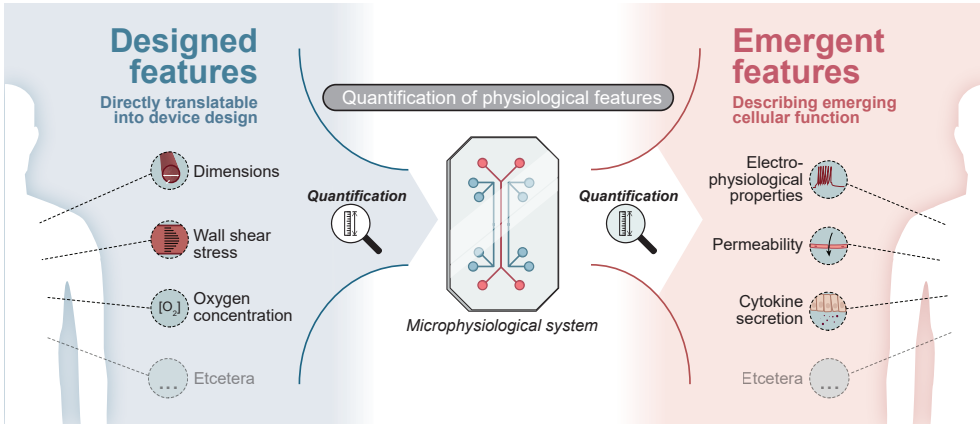

Figure 1: Microphysiological systems (MPS) can quantitatively control and monitor physiological features. *Two types of quantifiable physiological features can be distinguished: (1) 'Designed features' that can be controlled by chip design (e.g. compartment dimensions) or input (e.g. wall shear stress, oxygen concentration) and (2) 'Emergent features' that describe cellular function (e.g. electrophysiological properties, permeability, cytokine secretion) which develops as the combined result of design and biological responses of the cells inside the system. Features may belong to either or both groups depending on the specific model and functional read-out required.*

Quantification of physiological features in microphysiological systems of the vasculature, intestine, heart and brain and their in vivo relevance

In this section, we provide a comprehensive overview of quantifiable physiological features of the human vasculature, intestine, heart and brain, to provide deeper understanding of the elements required to create physiologically relevant and fit-for-purpose MPS. We describe examples of quantitative modeling of designed and emergent physiological features and compare these with values measured in humans *in vivo* (*Table 1*). The examples were selected because the quantification methods used and/or absolute values determined are most similar *in vivo* and in MPS; they can thus be used to assess the relevance of the model and benchmark certain physiological feature in MPS. Their value, for example for drug screening, would thus become evident for researchers and regulators alike. Quantified physiological features specific to a single organ are described in *SI Note 6*. Descriptions and an overview of the designed and emergent physiological features of the four selected organs are shown in *SI Note 2 and SI Figure 1*.

We report physiological features of the healthy state, not those specifically associated with any pathology, to ensure broad relevance in fit-for-purpose MPS applications. Although the ultimate goal of MPS is often modelling disease, these models themselves usually depend on cellular processes that also occur in physiological states. Quantifying "healthy" features, as in this review, provides a baseline for pathological values, which are often

abberant values of the same physiological features. The selection of organs is based on the developmental argument to include derivatives of all three germ layers: mesoderm (heart), endoderm (intestine), ectoderm (brain) and the blood vessels that link all organs in the body. We have covered a range of MPS per organ, for which the general design principles are shown in *Figure 2*. The majority of the systems discussed include microfluidics and are thus considered OoCs and referred to as Vessel-on-Chip (VoC), Gut-on-Chip (GoC), Heart-on-Chip

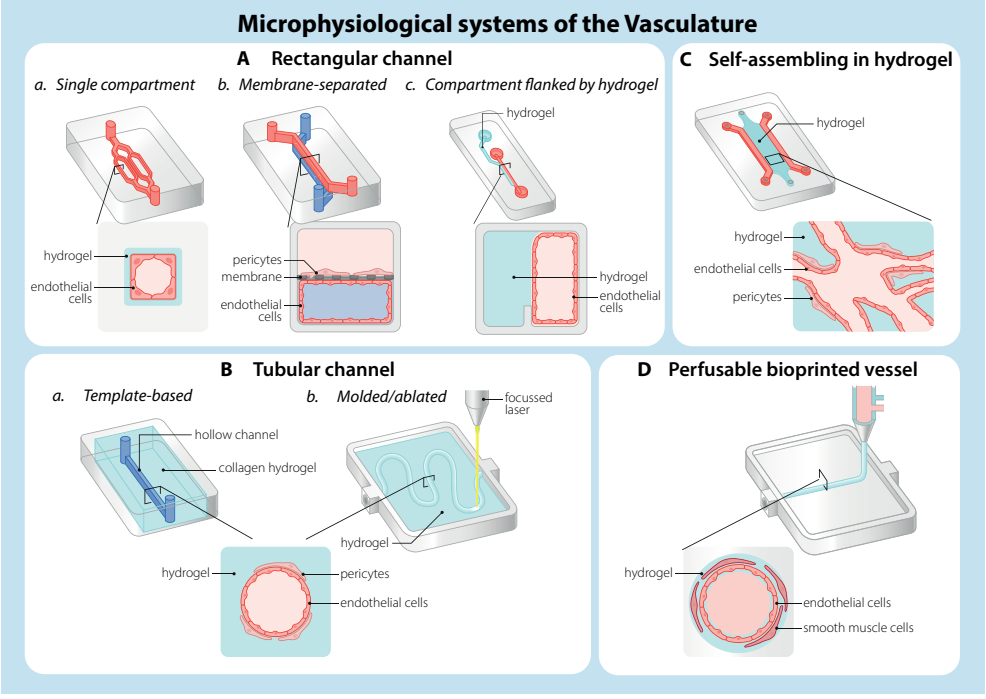

Figure 2: Design principles of different microphysiological systems of the human vasculature
Microphysiological systems of the vasculature: Aa) Single patterned channel, usually in PDMS although agarose gelatin hydrogel is also used. Widely used for mono-cultures of endothelial cells. Ab) Two aligned channels (upper and lower), separated by porous membrane. Unidirectional pressure-driven fluid flow can be introduced in both channels. The device is generated from PDMS, coated with a thin hydrogel layer. Cells can be cultured in both channels. The upper channel is usually seeded with tissue-specific cell types like astrocytes, neurons, lung- or intestinal epithelium and the lower channel with endothelial cells. Ac) Devices designed for use with gravitational bidirectional flow. Used in 2- and 3-channel formats. The side channel is used to seed endothelial cells and is flanked by a hydrogel-filled channel separated using a phase-guide. Tissue-specific cells can be seeded in the hydrogel channel. Ba) Tubular channels using templating are based on removing or replacing a structure within hydrogel. Examples include needle removal, or using differences in viscosity of fluids as in viscous finger patterning. A tubular structure remains which can be seeded with cells. Bb) Molding or laser ablation can create tubular structures within hydrogels in self-designed patterns. C) Self-assembly based systems make use of the vasculogenic capacity of endothelial cells: the ability to self-organize into vascular networks. Endothelial cells are usually mixed with mural cells, seeding in a hydrogel channel to enable development of a 3-dimensional (3D) vascular network. The hydrogel channel is usually flanked by media channels to enable network perfusion. D) Several tissue engineering approaches to bio-print vessel structures are available. One is printing cell-laden hydrogel within a predetermined structure.

Advanced 3D-printed structures are designed to connect to microfluidic set-ups after seeding. Aa) based on REF.[7] Ab) based on design by Emulate Inc, Boston, MA, USA and REF.[8] Ac) based on design by Mimetas, Oegstgeest, NL and REF.[9] Ba) based on REFs.[10,11] Bb) based on REF.[12,13] C) based on REF.[14–16] D) based on REF.[17,18]

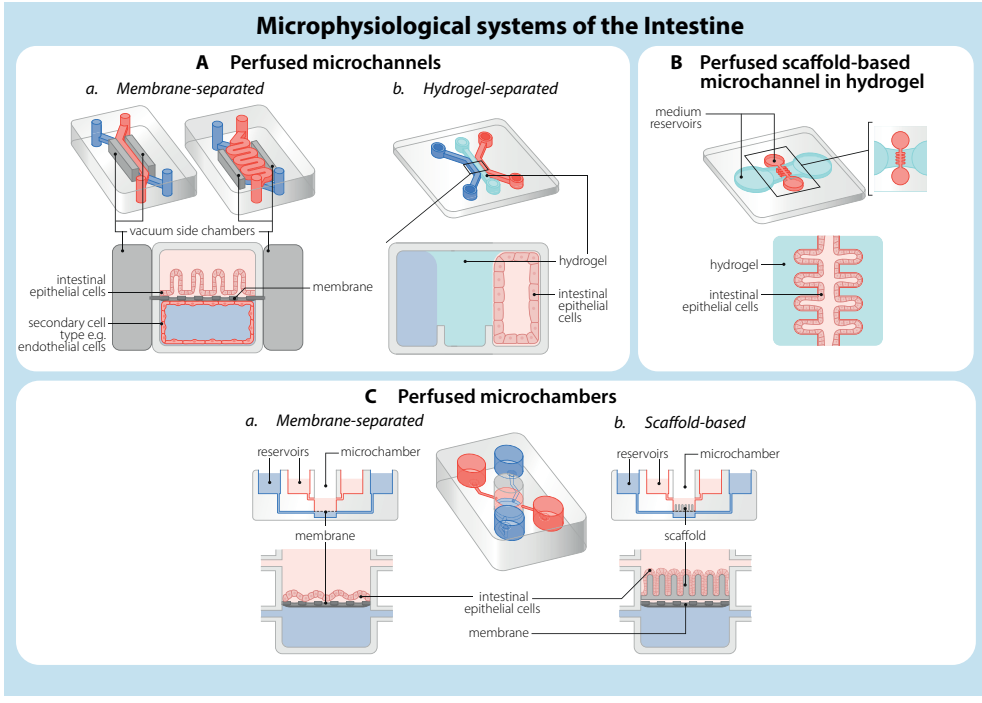

Figure 3: Design principles of different microphysiological systems of the human intestine
Microphysiological systems of the intestine: Aa) Two aligned channels (upper and lower), separated by porous membrane. Unidirectional pressure-driven fluid flow can be introduced in both channels. The device is made from PDMS, coated with a thin hydrogel layer. Cells can be cultured in both channels. The upper channel is usually seeded with intestinal epithelium and the lower channel with endothelial cells. The channel can either be linear, as on the left side, or bent, as on the right. Two smaller 'vacuum chambers' are parallel to the microfluidic channels and to pressurize and stretch the membrane and recapitulate peristaltic movement. Ab) Two aligned channels, separated by a hydrogel layer. Cells can be cultured in all three compartments (also within the hydrogel layer). Bidirectional gravitational fluid flow can be introduced to both channels. The device is made from plastic, coated with a thin layer of hydrogel. Ba) Two microchambers, separated by a porous membrane. Both compartments can be used for cell culture but the upper compartment is usually used. Pressure-driven unidirectional flow (peristaltic pump) can be introduced to both chambers. Bb) Two microchambers, separated by a porous membrane. A scaffold with villus-crypt architecture is located on the membrane. Both compartments can be used for cell culture but the upper compartment is usually used. Gravitational bidirectional flow can be introduced to both chambers. C) One tubular microchannel with villus-crypt architecture created in hydrogel by laser ablation. The device contains two separate media compartments (for perfusion of the microchannel lumen, from left to right, and in the hydrogel above and below the microchannel to create a gradient through the hydrogel). Cells can be grown in the microchannel or in the hydrogel. Unidirectional fluid flow (syringe pump) can be introduced to the microchannel.
Aa) based on design by Emulate Inc, Boston, MA, USA and REF.[19,20] Ab) based on design by Mimetas, Oegstgeest, NL and REF.[21,22] Ba) based on REF.[23] Bb) based on REF.[24] C) based on REF.[25]

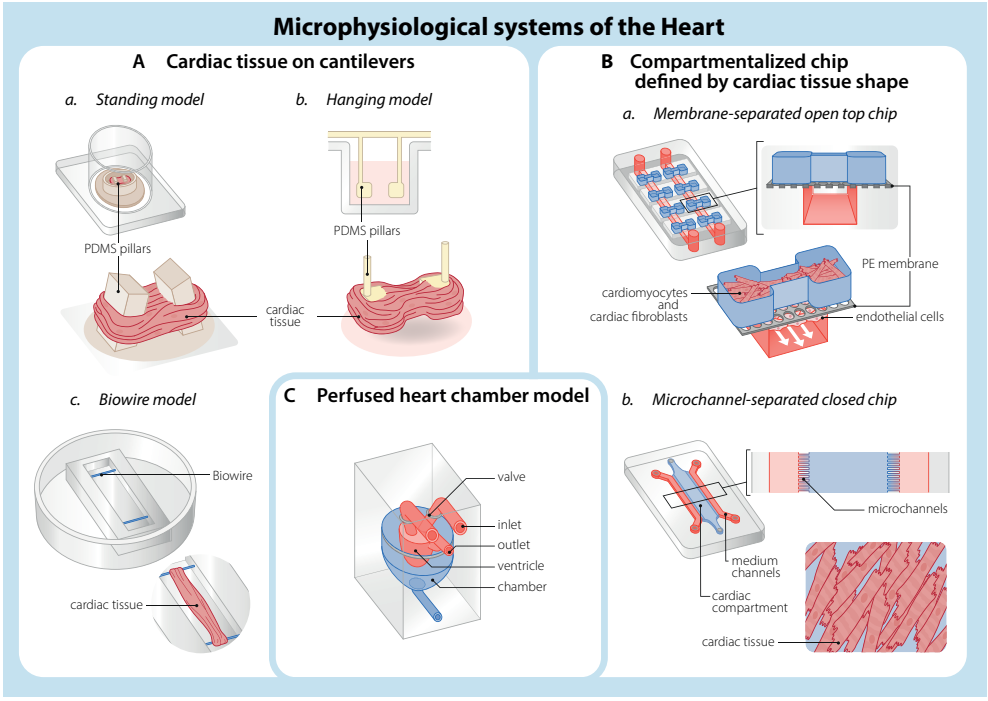

Figure 4: Design principles of different microphysiological systems of the human heart
Microphysiological systems of the heart: Aa) Standing rectangular micropillars made of PDMS that fit into 96-well plates. Ab) Hanging cylindrical pillars made of PDMS in a rack of 4 pairs that fit into 24-well plates. Ac) Patterned polystyrene sheets (Biowire). 3D-cardiac tissue is anchored to two horizontal wires within a chamber with two carbon electrodes that allow electrical stimulation. Ba) Open-top compartment system with "dogbone shaped" cardiac tissue on top, separated by a porous membrane. Lower channel is perfusable and can be used as an endothelial cell compartment. Bb) Cardiac tissue confined to the centre channel with side micro-channels to stimulate diffusion of nutrients from the flanking media channels. C) Polycaprolactone (PCL) / gelatin based heart chamber scaffold with input and output channels and a catheter for pressure and volume measurements.
Aa) based on REF.[26,27] Ab) based on REF.[28] Ac) based on REF.[29] Ba) based on REF.[30] Bb) based on REF.[31] C) based on REF.[32]

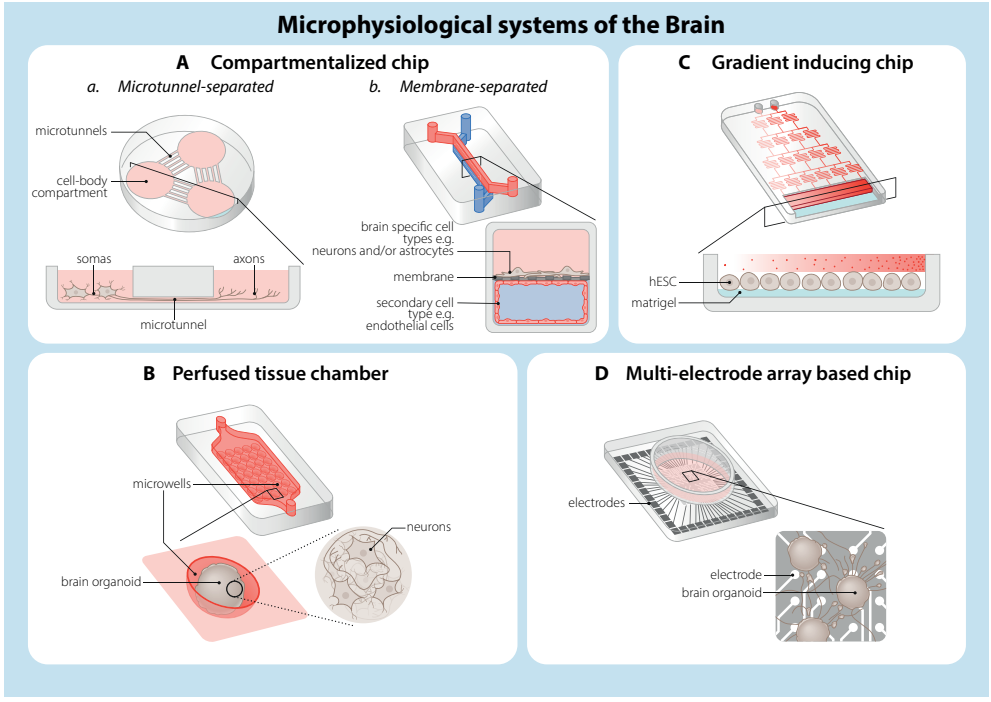

Figure 5: Design principles of different microphysiological systems of the human brain
Microphysiological systems of the brain: Aa) Specific cell-cell interactions in compartmentalized systems can be achieved through microtunnel or patterned devices. Here, the device has multiple culture compartments separated by microtunnels, resulting in physical separation of cell bodies of different cell types as they are unable to migrate but their protrusions can extend into a different compartment. Bb) Two aligned channels (upper and lower), separated by porous membrane. Unidirectional pressure-driven fluid flow can be introduced in both channels. The device is made from PDMS, coated with a thin hydrogel layer. Cells can be cultured in both channels. The upper channel is usually seeded with tissue-specific cell types like astrocytes or neurons and the lower channel with endothelial cells. C) Perfused tissue chambers containing microwells to enable culture of brain organoids, while creating interstitial flow. D) Gradient-inducing system created by sequential diffusive mixing of two inlet media, through which a linear growth factor gradient is established over the cell culture area. N) Multi-electrode array based systems have electrodes integrated into the device to measure the longitudinal development of electrophysiological network activity of for example neurons in vitro in real-time. Aa) based on REF.[33–35] Ab) based on design by Emulate Inc, Boston, MA, USA and REF.[8] B) based on REF.[36] C) based on REF.[37] D) based on REF.[38]

Designed features

We first describe physiological features that can be directly implemented and controlled in device design. We focus on how these features have been modeled and measured in an exemplary way in MPS of the vasculature, intestine, heart and brain and emphasize considerations that should be taken into account in comparing *in vitro* with *in vivo* measurements.

Table 1| Quantification of designed and emergent physiological features in microphysiological systems and human in vivo

	Category	Organ	Feature	MPS		In vivo (human)	Ref MPS	Ref In Vivo
				Method	Quantification	Quantification		
Designed	**Organ architecture**	Vessel	Tube diameter	Laser ablation	10-500 µm	Arteries: 0.03-2.5 cm, arterioles: 10-300 µm, capillaries: 5-10 µm, venules: 8-100 µm, veins: 0.01-2 cm	39	40
				3D biioprinting	700-1000 µm		17, 18	
		Intestine	Tube dimensions	Laser ablation	Diameter: 150 µm; length: 1200 µm; DLR: 0.125	Diameter: 2.5 cm (SI), 4.8 cm (LI); length: 300 cm (SI), 110-190 cm (LI); DLR: 0.008 (SI), 0.025-0.044 (LI)	24	41
			Crypt-villus dimnesions	Laser ablation	Crypt: diameter: 50-75 µm; depth: 170 µm; DDR: 0.29-0.44	Crypt SI: diameter: 50 µm; depth: 132-219 µm; DDR: 0.23-0.38. Villus SI: diameter: 132-165 µm; height: 273-720 µm; DHR: 0.18-0.60	32	42-44
		Heart	Ventricular chamber volume	Nanofibrous scaffold	500 µL	147 mL	33	45
		Brain	Regional connections	Compartmentalized system	Connection dentate gyrus - CA3 neurons within hippocampus	Separation of functional and structural neurons between and within brain regions	34	46
			Cortical layering	Compartmentalized system	Two cortical layers	Six cortical layers	34	47
	Fluid flow	Vessel	Wall shear stress	Various pump systems	Arteries: 1.2-1.5 Pa, arterioles: 0.42 Pa, capillaries/venules; 0.03-0.72 Pa, veins: 1 Pa	Arteries: 2.23 Pa, arterioles: 6-14 Pa, capillaries: 1.2 Pa, venules: 0.3-1 Pa, veins: 0.1-0.6 Pa	14, 48-51	52, 53
			Circumferential strain	Syringe pump	4-10%	5-10%	54	55, 56

	Category	Organ	Feature	MPS		In vivo (human)	Ref MPS	Ref In Vivo
				Method	Quantification	Quantification		
Designed	**Fluid flow**	Intestine	Wall shear stress	Pressure-driven flow	0.6-6 mPa	~0.2-8 mPa	19	19, 20, 57, 58
				Syringe pump	2 mPa		20	
		Brain	Cerebral spinal fluid flow	Miniature osmotic pump	0.15 µl/min	0.02-3 ml/min depending on brain structure	59	60
	Structural deformation	Intestine	Peristalsis	Vacuum chambers lining microchannel	Deformation: 0-30%; Frequency: 0.15 Hz	Deformation: 7.2-27.4% (SI); Frequency: 0-10 Hz (SI), 0.06-0.7 mHz (5-61/day) (LI)	19	58, 61
				Vacuum chambers lining microchannel	Deformation: 5%; Frequency: 0.15 Hz		20	
		Heart	Afterload	External magnets	0.61-5.40 mN/mm^2	8.31 mN/mm2 (human modelling)	62	62
		Vessel	Tissue elasticity	Tunable synthetic hydrogel	1-6 kPa	Arteries: 50-150 kPa, venous: 3-50 kPa (mouse)	63	64
		Intestine		Hydrogel	0.75 kPa	SI: 0.6–2.6 kPa, LI: 0.9 kPa	24	65
				Chemically cross-linked hydrogel	9.64 kPa		66	
		Heart		Varying acrylamide/ bis composition	1, 13, 90 kPa (soft, normal, stiff)	Fetal: ~1 kPa, adult: ~13 kPa	67	68
		Brain		Brain tissue-derived ECM	0.1 kPa	0.4 kPa	69	70
	Oxygen conentration	Vessel	Oxygen concentration	Oxygen scavenging channel	1-5%	1-13%	71	72

	Category	Organ	Feature	MPS		In vivo (human)	Ref MPS	Ref In Vivo
				Method	Quantification	Quantification		
Designed	**Oxygen concentration**	Intestine	Oxygen concetration	Integrated oxygen sensor	~0.3-1.5% (Gradient outlet-inlet epithelium channel)	Intestinal lumen: ~4-5% (SI), ~0.4-1.5% (LI)	73	74
		Heart		Hypoxic incubator	1, 5, 21%	5-10%	75	76
		Brain		Hypoxic incubator	5%	1-5%	8	77
Emergent	**Cell type diversity**	Vessel	Cell type diversity	scRNAseq	NA	ECs, SMCs, Pericytes, perivascular fibroblast, Mϕ (heterogeneous between tissues and along arteriovenous axis)	-	78
		Intestine	Epithelial cell diversity		50% SC, 30% ent, 5-10% dividing cell, 4-5% EEC, 2-3% PC, 2% M-like, 1% gob, 0.5-1% tuft	Ileum: 70-75% ent, 10-11% prog, 5% gob, 4-5% TA, 3-4% SC, 1-2% PC, 0-1% EEC. Colon: 35% prog, 20-22% gob, 15% ent, 12-14% TA, 8-10% PC, 3-4% SC, 0-1% EEC	24	79
		Heart	Cell type diversity		NA	30% cardiomyocyte, 24% fibroblast, 17% mural cell, 12% ECs, 10% immune cell	-	80, 81
		Brain			NA	10 major cell types, highly heterogenous between brain regions	-	82, 83
	Cell type localization and interaction	Vessel	Astrocyte coverage of endothelial layer	IF co-localization	9%	100% (rat)	84	85
			Pericyte coverage of endothelial layer	IF co-localization	16%	10-70% average all tissues, 30% BBB (rat)	84	85, 86

	Category	Organ	Feature	MPS		In vivo (human)	Ref MPS	Ref In Vivo
				Method	Quantification	Quantification		
Emergent	**Cell type localization and interaction**	Intestine	Epithelial cell type localization along crypt-villus axis	IF, fluorescence intensity along crypt-villus axis	Score from 0 (base) to 1 (top): proliferative cells 0-0.5, differentiated cells 0.5-1.	Score from -0.2 (base) to 1 (top): SC -0.2-0.2, goblet -0.1-0.3, EEC -0.1-0.3, enterocyte 0.1-0.9	87	88
		Brain	Regional specification	WNT gradient via microfluidics	Regional development along rostral-caudal axis	Regional development along rostral-caudal axis	36	89
			Synapse density	IF	2.2-2.6x103 synapses/µm2	8.6–12.9x108 synapses/mm3	90	91
			Neurotrans-mitter release and uptake	In-chip Electrochemical sensors	1-minute timescale	Millisecond timescale (mouse/ rat)	92	93, 94
	Inflammatory response	Vessel	Cytokine secretion	Luminex. Il-6	0.3 ng/ml	0.1 - 305 ng/ml	95	96
		Intestine		Multiplex assay, LPS, IFN-γ and TPCA-1 stimulated	Percentage of inhibition: Apical/Basal: IL-8 60%/70%, CCL-20 55%/70%, CXCL10 10%/50%	NA	22	-
		Brain		Membrane based antibody array	Upregulation of inflammatory cytokines	Upregulation of inflammatory cytokines	97	98
	Barrier integrity	Vessel	Permeability of the endothelial layer	Leakage assay 20 kDa	3x10-6 cm/s	2.4x10-7 cm/s (rat)	9	99
				Leakage assay 70 kDa	4x10-7 cm/s	1.5x10-7 cm/s (rat)	7	99
			Permeability of the epithelial layer	Fluorescent tracer leakage (4.4 kDa FD)	P-app: 7.12x10-6 cm/s	0.11-0.12x10^-6 cm/s (SI), 0.05-0.1x10^-6 cm/s (LI)	21	100

	Category	Organ	Feature	MPS		In vivo (human)	Ref MPS	Ref In Vivo
				Method	Quantification	Quantification		
Emergent	**Barriere integrity**	Intestine	Permeability of the epithelial layer	Rhodamine123 permeability	Influx: 5x10-6 cm/s, efflux: 1x10-6 cm/s	NA	25	-
				LC-MS: caffeine and atenolol	Caffeine: 34.5x10-4 cm/s, Atenolol: 3.8x10-4 cm/s	Caffeine: 2.93x10-4 cm/s, Atenolol: 0.2x10-4 cm/s	23	23
	Electrical signaling	Heart	Resting membrane potential	Patch clamp	-97 mV	-90 mV	101	102
				Impaling electrode measurement	-57 mV		103	
			Action potential amplitude	Impaling electrode measurement	97 ± 2 mV	102-110 mV	103	102
			Conduction velocity	Voltage-sensitive dye and optical-mapping	47.4 ± 12.4 cm/s	30-100 cm/s	104	102
		Brain	Electrical frequency	MEA	0.2 Hz to 3 Hz	0.05 Hz to 500 Hz oscillations	38	105
	Renewal	Vessel	Angiogenesis	Imaging	16 µm/h	NA	106	-
		Intestine	Epithelial turnover rate	EdU pulse-chase: 12h pulse, 10-day chase	4 days for full turnover	3.48 days (average entire GI epithelium)	24	58, 107
			Epithelial turnover rate	EdU pulse-chase: 24h pulse, 96h chase	40 µm/day	38-63 µm/day (SI, neonatal rat), 216/143 µm/day (Duodenum/ Ileum, mouse)	66	108, 109

Data was included based on the criteria as stated in Supplemental Information Note 1. Abbreviations: MPS=microphysiological system, NA=not available, ref=reference, SI=small intestine, LI=large intestine, DLR=diameter-to-length ratio, DDR=diameter-to-depth ratio, DHR=diameter-to-height ratio, ECM=extracellular matrix, GI=gastrointestinal, EC=endothelial cell, SMC=smooth muscle cell, Mϕ=macrophage, prog=progenitor cell, SC=stem cell, ent=enterocyte, gob=goblet cell, PC=Paneth(-like) cell, EEC=enteroendocrine cell, TA=transit-amplifying cell, BBB=blood-brain barrier, CRC=colorectal cancer, LC-MS=liquid chromatography-mass spectrometry, IF=immunofluorescence, scRNA-seq=single-cell RNA-sequencing, FD=fluorescein isothiocyanate-dextran, IL=interleukin, IFN=interferon, LPS=lipopolysaccharide, Papp=apparent permeability, m=meter, Pa=Pascal, Hz=Hertz, F=farad, V=voltage, N=Newton, h=hour, min=minute, s=second.

Organ architecture

Organ function is highly dependent on its organization and architecture. Stem cell based 3-dimensional (3D) self-organizing tissues, known as organoids, are able to recapitulate aspects of tissue architecture accurately but often suffer from heterogeneity and variability. MPS provide means to guide self-organization and control architecture using different technological approaches, like physical confinement or compartmentalization.

The vasculature and the intestine are essentially cylindrical tubes with diverging diameters (*Table 1*). To date, no single VoC has been designed that covers the entire range of true vessel diameters and most GoCs are at microscale and dimensions are not scaled accurately to the human intestine. VoC solutions for large structures like arteries and veins, that have both endothelial cells and smooth muscle cells, have been the main examples of OoCs converging with tissue engineering where pre-seeded 3D tissues, microfabrication and microfluidics are combined. For example, a new bio-compatible ink composed of alginate, gelatin methacrylate (GelMA), sodium alginate (SA) and glycidyl-methacrylate silk (SilkMA) was used to print tunable hollow microfibers, which could be attached to a microfluidic platform, providing a physiological, biocompatible microenvironment for cell adhesion and proliferation with dimensions comparable to *in vivo* (Table 1)[17]. VoCs with small diameters are either single tubular channel approaches, typically modeling vessels of 100-500 µm diameter, while self-assembled vascular networks in hydrogels result in vessels with diameters ranging from 10 to 500 µm[10,14,15,110]. However, these techniques either lack flexibility or diameters cannot be controlled. Laser photoablation has recently circumvented some of these issues. This technique allows high-precision patterning of lumenized structures in hydrogels using focused pulsed lasers[13,39]. This same technique is also suitable for GoC systems, generating perfusable tubular structures with 150 µm diameter containing crypt- and villus-like architecture in a hydrogel[24]. Even though the tube dimensions differ from the human intestine, the method shows promise for emulating intestinal architecture in a controlled manner. Moreover, in most cases it is not the intention to have models the exact size of the human intestine. For scaled *in vitro* model systems, more relevant dimensions are the diameter-to-length ratio of the intestinal tube and diameter-to-height or diameter-to-depth ratio of the villus and crypt respectively, of which the latter is comparable to the human small intestine in the earlier example.

The heart consists of multiple open chambers with specific geometries that are essential for building up the internal pressure necessary to pump blood through the body. Most HoCs do not model the entire geometry of the heart or its individual chambers but rather generate functional cardiac muscle tissues. Some HoCs have modelled the entire architecture or individual chambers either at a macro-scale or by scaling down to microtissue level. Steps towards macro-scale heart chamber geometries have been made by creating ellipsoidal nanofibrous scaffolds, compatible with microfluidic systems and exogenous pressure application, seeded with ventricular human induced pluripotent stem cell (hiPSC)-

derived cardiomyocytes[32]. Ultimately, the chamber geometry and volume is an important determinant of the forces generated on- and by the cardiomyocytes in these engineered chambers. A micro-scale multi-chamber microfluidic device has been developed with integrated sensors capable of measuring the pressure within the chambers. This pressure was induced by pneumatic membranes creating fluid flow in a closed loop covered with HUVECs, with four solenoid valves ensuring unidirectional flow through the four chambers[111].

For the brain, the most distinctive architectural feature is its spatial organization into different regions and the specific cellular layering within these regions. BoCs have been developed that mimic connections between- and within different mature brain regions by linking compartmentalized co-cultures containing different region-specific neuronal cell types (*Table 1*)[33,35] . On the other hand, mimicking the six neuronal layers of the cortex within these brain regions requires self-organization, which suffers from inherent variability, or compartmentalization of different cell types. This was achieved in a BoCs model using a PDMS stencil that created separate microchambers for seeding different neuronal cell types[34]. Although this BoC model does not completely mimic cortex development *in vivo*, the layered cellular architecture of the cortex can be recreated. In the future, combining these approaches for brain region specification and cellular layering could pave the way in recreating a full (micro)cortex.

These MPS examples describe the technical approaches being used to mimic physiological architecture. Importantly, as discussed for GoC, scaled-down versions of MPS are often practical in use but despite their size, can still be as biologically relevant. More extensive discussion of scaling in MPS technology is provided in the "Conclusion and Outlook" section.

Fluid flow

Organs in the human body depend on fluid flow to receive nutrients and immune protection and dispose of waste products. Different types of fluid flow can be distinguished: luminal fluid flow, discussed below, and interstitial flow, discussed in *SI Note 5*.

Luminal fluid flow exerts mechanical forces on cells in the tubular wall and is proportional to the local fluid flow rate, local lumen geometry and the viscosity of the fluid. The resulting wall shear stress (WSS) is sensed by the cells and transduced into biological responses such as altered permeability and cellular remodeling. In the vasculature, large internal pressures in combination with wall elasticity result in circumferential strain as an additional force on these cells. Several microfluidic solutions allow establishment of physiologically relevant fluid flow in OoC devices. The highest flow rates in the body are in the arteries. This can best be replicated using peristaltic piezoelectric pumps as they can produce pulsatile flow with high flow rates because of their inherent high frequency output. This was demonstrated experimentally using a piezoelectric braille-pin system to actuate a peristaltic pump that induced high flow rates (30 mm/s) corresponding to up to 1.2 Pa of WSS on endothelial cell cultures[48]. As seen *in vivo*, endothelial cells align and elongate

with increasing flow rates. Pneumatic systems are also used because of their high force output which supports tunable high flow rates. It was shown for example that in hiPSC-derived endothelial cells, arteriovenous specification, quantified by arterial and venous marker expression, could be controlled in a microfluidic set-up with six parallel cell culture chambers with shear stresses of up to 1.5 Pa[49]. Arteriole-like flow profiles and flow rates can be achieved in various microfluidic systems, as long as they have pulsatile flow options. For example, a microfluidic heart-like valve was developed using a pressure system that could reproduce pulsatile flow accurately[50]. While this approach is promising, 0.42 Pa was the maximum achievable WSS, lower than that *in vivo*. Capillaries and venules both require low flow rates with laminar profiles inside a channel just a few microns in diameter. These requirements can be fulfilled in multiple ways. Hydrostatic pressure is one that is easy to use where low flow rates can be approximated by addition of different volumes of media in the microfluidic reservoirs of a device[14]. One disadvantage of this approach is the varying flow rate, and thus WSS, over time. For modeling veins, pressure-driven pumps are preferred since they reproduce a steady non-pulsatile pattern with high flow rate. This was exemplified in a study of the alignment of human umbilical vein endothelial cells (HUVECs) upon recirculation flow at shear stresses up to 1 Pa[51]. Pressure-driven pumps are also commonly used to model the luminal fluid flow in GoCs. One of the first GoCs, developed by the Wyss Institute, used this technique to expose the cells to a physiologically relevant WSS ranging from 0.6 to 6 mPa depending on fluid flow rate[19]. Of note, to simplify the design, most VoC and GoCs model the organ as a straight cylindrical or rectangular microchannel, thereby neglecting the irregular turns that can profoundly impact flow profiles in reality[112]. Recent work accounted for this in a GoC model that integrated a non-linear asymmetric flow profile allowing more precise representation of *in vivo* intestinal flow (*Table 1*)[20].

Importantly, even though various technologies now support integration of physiologically relevant flow profiles in *in vitro* models, it is essential to verify the biological relevance of the resultant forces for the resident cells. Reporting WSS, instead of absolute fluid flow rate, provides a single measure that can be used to compare OoCs with human physiology since it takes into account channel geometry, fluid properties and flow parameters. Accurately modeling circumferential strain remains technically difficult, however, recent advances such as the use of a template-based tubular VoC coupled to a syringe pump, allowed mimicking of physiological values (*Table 1*)[54]. Future modelling of circumferential strain could be further improved by using new piezoelectric materials (see 'Technical advances' section).

Structural deformation

Many organs contain muscle cells that structurally deform the tissue. MPS exploit several principles to induce these types of structural deformation and strain on cells. Several GoC systems include vacuum chambers flanking the microchannels that cause rhythmic

membrane deformation through cyclic suction to mimic peristalsis. This approach can generate physiologically relevant deformation ranging from 0-30% at 0.15 Hz frequency[19]. One recent GoC system displayed a non-linear bent channel, in which the flanking vacuum chambers induce multiaxial cellular deformation, rather than the biaxial deformation of linear microchannels. This better reflects complex human intestinal movement at both macroscopic- and microscopic (villus motility) levels (*Table 1*)[20]. Whereas muscle cells are absent in these GoC models the device design replaces muscle cell function. For MPS of the heart the design is used to stimulate and optionally control the contraction of (cardiac) muscle cells in the system. In this way, the design allows modelling of specific states of heart (or intestinal) contraction, such as afterload, a period of systolic contraction when cells are exposed to increased strain to pump against arterial pressure, or cyclic stretch. Cantilever-based Engineered Heart Tissues (EHTs) mimic afterload by organizing the cardiac tissues around pillars or micropoles on a flexible membrane to pneumatically increase the strain[113]. Alternatively, EHTs can contain small magnets controlled by a piezoelectric stage to modify afterload dynamically *in vitro*[62]. Further work implementing precise control of actuation and stimulation in MPS is ongoing using piezoelectric materials and ionic polymer-metal composites (see 'Technical advances' section).

Tissue elasticity

Tissue elasticity influences many cellular responses and is often altered during disease as a result of fibrosis. Most cell types react to changes in mechanical properties of ECM by converting mechanical cues into biological responses. Changes in ECM elasticity can convert differentiation in endothelial cells to pathological angiogenesis[64], cardiomyocyte maturation to heart failure[114], intestinal stem cell expansion to cancer progression[65] and alter neuronal differentiation, wiring and plasticity[70].

Tissue elasticity, described by the elastic modulus (E in Pascal) varies per organ in the human body from less than 1 kPa for some soft tissues like the brain and over 10 kPa for muscle tissues[70]. Conventional *in vitro* experiments are often carried out on glass or plastic which is too stiff (in the GPa range). Commonly used alternatives are very soft natural hydrogels such as collagen, fibrin or Matrigel (<1 kPa)[115,116]. Many MPS devices are composed of stiff materials, such as PDMS (0.8-4 MPa)[117], coated with a thin layer of ECM. Since this does not accurately reflect soft tissue elasticity *in vivo*, natural hydrogels have been used to generate softer scaffolds within these systems. One GoC model used laser ablation to create a microchannel in polymerized hydrogel containing neutralized collagen and Matrigel, resulting in an elastic modulus of 0.75 kPa[24]. This approach led to successful generation of a perfusable microchannel containing villus-crypt architecture. Another way to model soft tissues is to use decellularized human tissue-derived ECM, as shown for a microfluidic BoC system. This provided not only physiologically relevant elasticity but also the wide range of biologically relevant components within the ECM. The model

showed improved cortical layering and electrophysiological function of hiPSC-derived brain organoids[69]. The obvious drawback of this method is the need for human tissue for ECM-derivation, although potential was shown for porcine-derived ECM. Most other tissues, including certain parts of the intestine, have tissue elasticities greater than 1 kPa and thus require modified- or alternative hydrogels. Moreover, as these natural hydrogels are too soft to generate standing structures, stiffer materials are necessary for some applications. One approach is to cross-link natural hydrogels, exemplified by a non-perfused scaffold-guided intestinal tissue model that used chemically cross-linked collagen to increase the hydrogel elasticity to 9.46 kPa[66]. This allowed molding of the hydrogel (via a PDMS stamp) into standing micropillars and microwells that mimicked the architecture of the human small intestine. Alternatively, tunable synthetic hydrogels can be used. These have been shown to be able to mimic the stiffened substrate of the heart during fetal (1 kPa), normal (13 kPa), and diseased (90 kPa) states in 2D[67] and for modeling angiogenic sprouting with physiologically relevant elasticity (1-6 kPa) in 3D (*Table 1*)[63].

As shown in the examples above, using the right elasticity for MPS remains a balance between ease-of-use and biological compatibility. Future approaches could resolve these issues: for example, new materials, like soft thermoplastic elastomers and chemically enhanced versions of PDMS, are being developed that allow tuning of the elasticity in 3D-cultures and can be used in standard fabrication methods, such as injection molding, hot embossing, 3D printing or micromachining (*Table 1*)[118–120]. In addition, 'smart materials' could be used to quantitatively manage the mechanical properties more accurately, for example based on response to pH variation, ion concentration, temperature, electric field[121,122].

Oxygen concentration

The vasculature, intestine and heart have unique oxygen profiles that display steep gradients from one region to the other. Most MPS devices are made of gas-permeable polymers such as PDMS and cultured in standard cell culture incubators with supraphysiological oxygen conditions (21% O_2). Several MPS approaches are available that mimic the *in vivo* oxygen concentration more closely. The most straightforward is placing the PDMS device in an anaerobic incubator. For example, a BoC/VoC-device that models the blood-brain-barrier (BBB) has shown that development under hypoxic conditions (5% O2) improved the formation of this barrier, resulting in higher impedance between microfluidic chambers and selective shuttling of drugs and antibodies[8]. Similarly, HoC devices, containing human 3D-cardiac tissues, were placed in environmental chambers with varying oxygen concentrations (1%, 5% and 21%)[75] to study hypoxia, which is crucial in myocardial infarction and to mimic the fibrosis that follows heart damage. While no differences in viability were seen across the different levels of oxygen, the myofibroblast marker, α-smooth muscle actin, was upregulated and contractile function was impaired. Actively perfusing a system in an oxygen controlled environment can create aerobic and anaerobic compartments within the same device. This

is well-suited for a PDMS-based GoC device placed in an anaerobic chamber, perfused with deoxygenated medium in the top channel and oxygenated medium in the bottom[73]. This created an oxygen gradient that ensured survival of both the anaerobic micro-organisms in the top channel and the human epithelial cell layer growing on the membrane separating the top and bottom channel. Integrated sensors allowed real-time measurement of oxygen tension. Physiologically relevant oxygen concentrations were thus reached (below 0.3% in the epithelial channel; ~10% in the endothelial channel), which supported maintenance of complex human microbial cultures for five days. The same system can be used to create oxygen gradients along the length of the luminal chip channel. A more subtle solution for creating physiologically relevant oxygen concentrations in MPS was shown in a VoC where temporal and spatial regulation of oxygen distribution was achieved in a hydrogel culture chamber by using an oxygen scavenger in the adjacent microfluidic channels[71]. This resulted in controlled and easily adjustable oxygen concentrations within the physiological range of 1-5% and allowed the study of angiogenic bias to hypoxic environments (*Table 1*). In the future, a new generation of polymers for device fabrication with lower permeability to oxygen hold great potential for MPS devices to approximate physiologically relevant oxygen concentrations without using an anaerobic chamber or oxygen scavengers (see 'Technical advances').

Emergent features

This section describes physiological features that develop as a consequence of device design, microenvironment and functional cell type, and can be measured as a system read-out. We focus on how these features have been modeled and measured quantitatively in MPS of the vasculature, intestine, heart and brain and emphasize considerations that should be taken into account in comparing *in vitro* with *in vivo* measurements. The quantified emergent features that are specific to a single organ are described in the *SI Note 6* and include cellular contraction for the heart, microbiome diversity, mucus layer thickness and digestion and absorption for the intestine and neuron-specific morphological features that support electical signaling for the brain.

Cell type diversity

Proper organ function relies on the presence of diverse, often organ-specific, cell types. Most MPS studies only quantify cell-type ratios as input into the system; however, the seeding composition does not necessarily reflect the cell-type diversity at the time that functional read-outs are made, since this will be influenced by the system microenvironment and whether the cells proliferate differentially. Quantification of cell type diversity at the time of read-out is essential for comparing different *in vitro* systems and investigating *in vivo* relevance.

Most MPS studies quantify different cell types by immunofluorescent staining,

which provides insight into both cell type diversity and localization but is limited to established markers and is difficult to quantify. Single-cell RNA sequencing (scRNAseq) is an emerging technique able to quantify cell type diversity in an unbiased manner. A recent GoC study used scRNAseq to provide an unbiased quantification of the intestinal epithelial cell type diversity[24] (*Table 1*). As an example, but also an exception, we have included this analysis based on intestinal epithelial cells from mice, as it shows the potential of scRNAseq in this context and the identification of rare cell types. However, it would be interesting to use the same technique to quantify intestinal epithelial subtypes of human origin in a GoC system and compare to human *in vivo* data. Aside from brain organoid scRNA studies, there is also a BoC scRNAseq dataset from brain region-specific neurons; however this focussed only on early stage progenitors and neurons and was far from recapitulating the full range of cells found in the adult brain[36]. Although scRNAseq has already been used to investigate cell type diversity of the adult vascular tree and heart *in vivo* (*Table 1*), it has not yet been used to assess this diversity in MPS. Current VoC systems remain unable to model the full complexity of the vascular tree and have therefore not yet been investigated for heterogeneity in much detail. Most HoC approaches use a combination of cardiomyocytes and fibroblasts, in a typical 4:1 ratio. In addition, certain devices have been fabricated to facilitate specific cellular niches such as a bilayer membrane microfluidic chip which allowed initial separation and transmigration of endothelial cells to the cardiac compartment[123]. However, for both types of HoC devices, cell heterogeneity and comparison to *in vivo* has not yet been assessed.

Cell type localization and interaction

Tissue functionality not only depends on cell type diversity but also on the location of cells within a tissue and their interaction with each other. Spatial organization and co-localization of different cell types can provide insight into tissue-specific micro-environments and intercellular communication These features have been quantified in different MPS using immunofluorescent staining and microscopy.

A study using a non-perfused scaffold-guided intestinal tissue model described an elegant manner to quantify the spatial organization of intestinal epithelial subtypes along the crypt-villus axis[87]. It was possible to control the distribution of different intestinal epithelial subtypes by creating growth factor gradients. Immunostaining that distinguished 'proliferative' and 'differentiated' epithelial populations was used to quantify their abundance and location along the crypt-villus length. A similar approach was used to characterize the developing human intestine *in vivo*[88]. This approach can be used in GoC models independent of whether tissue is scaffold-guided or self-organized and it allows almost direct comparison with the human intestine *in vivo* (*Table 1*). In a similar way, the spatial organization of neurons was modelled in a BoC system. The system incorporated microfluidics to mimic the growth factor-gradient along the rostral-caudal axis of the neural tube *in vivo*[36]. This allowed

microfluidic-controlled stem cell differentiation and regionalization, resulting in spatially organized neuronal subpopulations, much like those seen during human brain development

Besides using fluorescent read-outs to quantify cell localization, fluorescence also allows co-localization of different cell types to be studied, indicating possible cell-cell interaction. This method was used in a self-assembling VoC/BoC system of the BBB to quantify coverage of the endothelial abluminal side by both pericytes and astrocytes using maximum projection images of confocal z-stacks[84]. Similarly, the formation of synaptic connections in neuronal cells has been quantified in a BoC with two lateral chambers connected by a central channel through an array of microgrooves. This allows controlled quantification of dopaminergic synapses in the central channel by fluorescent labelling of pre- and post-synaptic markers[90]. However, this quantification was done on a z-projection of a 3D chip culture area; it is therefore challenging to directly compare with numbers in the human cortex which were quantified as the number of synapses per volume (*Table 1*). The potential for a more functional way of quantifying cell-cell interaction in neuronal synapses was exemplified in a BoC system that applied high-temporal resolution electroanalysis of neurotransmitter homeostasis *in vitro*[92]. The dynamics of dopamine uptake and release were quantified by continuous monitoring in human neuroblastoma cells using electrochemical sensing in a microfluidic device. Using this approach, it was possible to monitor kinetics on a 1-minute timescale *in vitro*, as an indirect measure of synaptic responses that occur in much shorter timeframes (~250 msec) (*Table 1*)[94]. A future improvement in quantification of cellular interactions and organization is spatial transcriptomics, which provides an unbiased quantification of cell type diversity and localization in both MPS and primary tissue[124,125], or microwave technology for analysis in real-time which may provide even more precision (see 'Technical advances' section). Besides quantification of cell co-localization in MPS, functional read-outs are necessary to confirm actual cell-cell interactions within a model system, as exemplified for synaptic interactions in BoCs.

Inflammatory response

All organs contain immune cells that surveil the tissue and determine when tolerance or an immune response should occur. An inflammatory response can be elicited to protect the body from harmful pathogens through a complex cascade of cellular interactions. This cascade involves the recruitment of circulatory- or tissue-resident immune cells into the affected tissue and is mediated by the secretion of cytokines as means of intercellular communication. Quantification of the number of transmigrated or infiltrated immune cells (discussed in *SI Note 6*) and cytokine secretion are thus clinically relevant proxies for the inflammatory and disease state[126].

Cytokine secretion can be quantified in serum or blood samples, in principle enabling direct comparison of *in vivo* with *in vitro* concentrations within the vascular system. One VoC system which used this quantitative approach showed physiological

levels of interleukin (IL)-6 (*Table 1*)[127]. However, as cytokine production is local and context-dependent, systemic measurements in body fluids might not reflect concentrations *in vitro* and should be viewed rather as useful indicators. In order to compare cytokine secretion in MPS with different dimensions, normalization to cell number and media volume is required. An alternative is normalization to endothelial cell area, as was done in a template-based tubular system of the BBB[95]. Sampling internal fluids of different organs, such as the intestine, brain and heart, is often not possible, making direct *in vivo* to *in vitro* comparison challenging. One way to address this is to study relative changes in cytokine levels upon exposure to reference compounds (e.g. drugs) that have been studied extensively *in vivo.* This approach was shown to be effective in a GoC model containing two hydrogel-separated perfusable microchannels, one of which was seeded with primary intestinal epithelial cells. Cytokines were measured in the supernatant after stimulation with lipopolysaccharide (LPS) and interferon gamma (IFN-y) to mimic inflammatory bowel disease (IBD)[22]. TPCA-1, a known anti-inflammatory compound *in vivo*, was shown to reduce this proinflammatory cytokine production of intestinal epithelial cells in a dose-dependent manner. This was more pronounced for basolateral production than apical, underlining the location-specific cytokine fluctuations and the relevance of having access to both sides of polarized cell layers in MPS. Cytokine secretion has also been measured in a 3D multi-cellular BoC-device to study neuroinflammatory responses[97]. The model consisted of hiPSC-derived neurons and astrocytes, grown together with primary human microglia. The activation of microglia was confirmed by the presence of pro-inflammatory cytokines in the culture medium. This model would be valuable to study relative changes induced by drugs or other reference compounds, as done for GoCs.

Since the inflammatory response is a feature that is often used in clinical diagnosis, the comparison of MPS and human observations is valuable for disease modelling and drug discovery. As shown here for selected examples, data from MPS can increasingly be compared directly with clinical outcomes. However, attention is still required for the quantification methods, units and scaling of the model system. If direct comparison is not possible, analysis of relative changes induced by reference compounds that are well-established *in vivo* will be essential to benchmark MPS.

Barrier integrity

The body has several organs that act as selective barriers to regulate transport of nutrients, while protecting tissues from toxins. In the vasculature and intestine, this selective barrier is formed by the combined effect of tight- and adherens junctions between endothelial and epithelial cells, respectively, and the basement membrane. The intestine, as one of the mucosal tissues in the body, has an additional layer of protection from the environment: a layer of mucus covering the epithelial luminal side (discussed in *SI Note 6*).

The integrity of the barrier, for both mucosal and non-mucosal barrier tissues, is

often quantified *in vitro* or *ex vivo* by one of two methods: transendothelial/transepithelial electrical resistance (TEER) or fluorescent tracer leakage. TEER is often used in MPS but may show inconsistency across- or within models. Considerations on quantifying barrier integrity using TEER in a reliable way are given in the 'Technical advances' section. Leakage assays are somewhat easier for use in MPS as compartmentalization and controlled cell area for diffusion allow good reproducibility and standardization. One of the most intensively investigated barriers using this technique is the highly selective and therapeutically important BBB. BBB models are usually based on a standard VoC system to which various types of brain cells are added, most commonly astrocytes, resulting in similar quantification methods for both. Absolute values of solute permeability *in vivo* have been mimicked with a range of VoC models[128]; however, some systems remain more suitable than others for direct *in vivo* comparison. It is important that designed features influencing permeability, such as vessel geometry and flow rate, are standardized. This favors rectangular and tubular microchannel VoCs over self-assembling vascular networks with higher diameter variability. For example, standard diameter microchannels under continuous unidirectional flow that were suitable for long-term assessment of endothelial cell permeability indicated 70 kDa permeability (4×10^{-7} cm/s), which is similar to rat vessels *in vivo* (*Table 1*)[7]. Application of unidirectional flow still requires more complex microfluidic set-ups, generally limiting the throughput of permeability measurements. One solution, which has been used for both VoC and GoC systems, is based on microtiter format plates that incorporate bi-directional flow and allow real-time monitoring of fluorescent tracer leakage into a hydrogel lining the tissue channel[9,21]. Distinct fluorescent tracers can be used to quantify bi-directional permeability of a barrier, as they are transported through passive paracellular absorption in the influx direction and carrier-mediated transport in the efflux direction, as was shown for rhodamine 123 in a perfused GoC microchamber [25,129].

Whilst fluorescent tracers are valuable in comparing permeability of different model systems and *ex vivo* data, for comparison with human tissues *in vivo* it is essential to have a set of reference compounds for which translocation properties in humans are known, such as food-derived components or drugs. This was exemplified in a GoC study which described apparent permeability values of two reference molecules, caffeine and atenolol, with well-known transmucosal permeability *in vivo*[23] (*Table 1*). This can be advanced by the integration of electrochemical sensors in devices allowing real-time measurement of a diverse range of compounds in OoC flow-through with high sensitivity, as detailed in the 'Technical advances' section'.

Electrical signaling

Multiple tissues in the human body use electrical signals to propagate functional information from cell to cell. In the brain, electrical signals orchestrate neuronal communication, while in the heart they are key for muscle contraction. These electrical signals are the result of highly

temporally regulated flow of ions across the plasma membrane of individual cells. While this basic mechanism is conserved, the architecture and function of the different organs has evolved such that these cells have very distinguishable features; this is discussed specifically for the brain in *SI Note 6*.

The specific morphology of electrically active cells results in efficient conduction of membrane currents. The conduction velocity of these currents within tissues depends on cell geometry and spatial patterning of the gap junctions which connect neighbouring cells[130]. Since PDMS is transparent, voltage-sensitive dyes can be used to measure conduction velocity in 3D tissues. One study using a pillar-based EHT model found that the conduction velocity in human embryonic stem cell derived-cardiomyocytes was comparable to that of healthy human heart (*Table 1*)[104]. Other electrophysiological parameters, such as resting membrane potential, action potential and excitation threshold are dependent on the abundance and localization of ion channels in the cardiomyocyte- and neuronal membranes[131,132]. Measuring these features *in vitro* involves impaling single cells with a glass electrode in a method referred to as whole-cell patch-clamp[133]. Similar (external) techniques are being used to assess the electrical activity of cells in MPS. For example, using 3D-cardiac tissue with standing pillars, impaled electrodes showed the resting membrane potential was slightly lower than physiological but the action potential amplitude was about 97±2 mV, close to that in mature cardiomyocytes[103] (*Table 1*). Sharp electrode measurements showed that hiPSC-derived cardiomyocytes from dissociated cardiac bio-wire models had similar resting membrane potentials (-97 mV) to adult human cardiomyocytes. Nevertheless, these types of measurement remain low throughput and technically challenging while it would be beneficial to integrate electrical readout in the devices for continuous readout. One alternative with greater ease-of-use and continuous electrophysiological measurements are multielectrode arrays (MEAs). In MPS of the heart, MEAs have been integrated in flexible and patterned PDMS membranes allowing measurement of electrical activity in aligned myocardium to which mechanical strain can be applied to the monolayer simultaneously[134]. For MPS of the brain, 3D high-density MEAs have been developed to measure the dynamics in 3D brain organoids at cellular resolution[135]. Measurement of brain organoids on MEAs revealed complex oscillatory waves that mimic activity in preterm neonates[38]. Highly synchronous events were detected at 0.2 Hz burst frequency and 3 Hz local field potential, much like those *in vivo* (*Table 1*). New developments include MEAs made of flexible, optically transparent electrodes poly(3,4-ethylenedioxythiophene) polystyrene sulfonate (PEDOT:PSS)-based polymeric electrodes, which allow simultaneous imaging of cells and measurement of electrical field potential[136], and the integration of flexible 3D electrodes into MEA platforms for spatial mapping across 3D tissue volumes[137]. Alternatives to these traditional electrophysiological measurements are high-frequency imaging using voltage- and calcium-sensitive dyes or genetically-encoded voltage- (GEVI) and calcium (GECI) indicators. These permit continuous monitoring of electrical activity in cell cultures, while

avoiding terminal endpoint measurements[138].

Renewal

Turnover and cell renewal rates vary greatly per organ. The intestine has one of the highest turnover rates and cells are replaced continuously, whilst the heart and brain have very little regenerative capacity[139]. The vasculature also has a relatively slow and location-dependent turnover rate but retains the capacity for wound healing and the formation of new blood vessels from existing ones (angiogenesis) after, for example, damage.

Intestinal epithelial cells undergo directional migration from the crypt to the villus tip to sustain the high turnover rate. This process has been studied in perfused tubular scaffold-based GoCs using 5-ethynyl-2'-deoxyurinidine (EdU) pulse-chase to monitor cell division over time[24]. Four days after the EdU pulse, all labelled cells had been shed into the luminal space and none remained in the epithelial layer, marking full-turnover, in line with the turnover rate of the human intestine. Of note, the distance cells travel from the crypt to the villus tip in GoCs is often not representative of the distance travelled in the human intestine. Therefore, an alternative approach would be to quantify the migration speed of the epithelial cells. This was measured using the same EdU pulse-chase method to be 40 µm/day in a non-perfused scaffold-guided intestinal tissue model[66], which falls within the range measured in neonatal rat small intestine but is lower than values in mice (*Table 1*). A reference value for the human intestine has not been reported to our knowledge. Via similar immunostaining techniques, the migration of endothelial cells during angiogenesis was studied in VoC models. Since angiogenesis is often disease- or development-related, extrapolating *in vivo* values to benchmark *in vitro* assays is challenging. VoC models however do provide opportunities to study which parameters might influence the process. One such model consists of multiple parallel microfluidic channels which can be filled with either hydrogel or culture medium to investigate how mechanical cues, like interstitial flow modulated by hydrostatic pressure differences over the channels, affect angiogenesis (*Table 1*)[106]. Immunofluorescent imaging was used to quantify sprout number, length and nuclear translocation within the sprouts at different timepoints. Another study quantified sprout formation kinetics using fluorescently tagged vascular and lymphatic endothelial cells in two parallel microchannels to investigate vascular and lymph angiogenesis in the same hydrogel[140]. Quantitative comparison of angiogenesis in these VoC systems would benefit from consistent reporting of angiogenesis in µm/hour.

Technical advances to improve quantification of physiological features in microphysiological systems

As evident from the previous sections, quantitative control of physiological features is still limited in MPS. This is in part due to lack of awareness on how important it is to report quantitative data and refer them to *in vivo* physiology. In addition, however, many quantitative

culture parameters are impossible to engineer or measure in the current generation of MPS. In the following section, we describe upcoming technologies which could improve or enable quantification in one or multiple organ model systems.

Designed features

Technical advances in device design could lead to better approximation of the tissue environment or architecture to that *in vivo* or improve quantitative control of physiological features (*Figure 6*).

Materials

MPS materials can profoundly impact the control of features as they dictate biocompatibility, stiffness, optical transparency, gas permeability, absorption of small molecules, manufacturability and reliability of the devices. PDMS is the most common elastomer used to manufacture MPS; however, despite many advantages, PDMS shows hydrophobic recovery[141], high and non-specific absorption of small hydrophobic molecules[142], and high gas permeability[143,144], which challenges the control of some physiological features. For instance, maintaining hypoxia or an oxygen gradient in VoCs and GoCs requires tight regulation of oxygen concentration. In addition, PDMS may interfere with establishing growth factor gradients or measuring secreted molecules (e.g. neurotransmitters, cytokines, metabolized drugs). Alternatives to pristine PDMS include PDMS-based elastomers with tailored long-lasting bulk[145] and surface[146,147] hydrophilicity, thermoplastic elastomers (sTPE) and off-stoichiometric thiol-ene (OSTE) polymers. sTPEs are biocompatible, optically transparent, and amenable to high throughput fabrication (e.g. by injection moulding) since they combine the properties of thermoplastics and elastomers[148]. Importantly, sTPEs show lower small-molecule absorption[149] and oxygen permeability than PDMS (2-50 Barrer versus 500 Barrer)[150]. OSTE polymers are also optically-transparent elastomers featuring lower small-molecule absorption and more stable surface modification capabilities than PDMS, and a wide range of stoichiometry-dependent stiffness[119]. The lower oxygen permeability of both materials enables better modeling of hypoxic conditions in vessels and intestine without needing anaerobic incubators.

Actuation and stimulation

Stimulation and actuation in MPS are important to mimic the dynamic microenvironment in some organs. Examples of actuation are mimicking the peristaltic movement in the intestine, recreating circumferential strain in the vasculature, or modeling of the strain seen in the beating heart.

Piezoelectric materials can be used for actuation of tissues within MPS. Unlike piezoresistive materials commonly used for strain sensing[151,152], piezoelectric materials can transduce electrical signals to mechanical movement and reciprocally sense mechanical

motion to convert it to an electrical signal. They can thus be used as both micro-actuators and sensors in MPS. Piezoelectric cantilevers have been used to electrically induce mechanical bending; additionally, when hiPSC-derived cardiomyoctyes were cultured directly on the cantilevers, their contraction dynamics and alterations upon drug exposure could be sensed by the cantilevers[153]. To a lesser extent, certain types of electro-active polymers also show reciprocal transduction between mechanical and electrical signals. Ionic polymer-metal composites (IPMCs) represent one such type of polymers, which in turn offer higher biocompatibility and softness than typical piezoelectric materials[154]. Additionally, IPMCs benefit from hydration with solutions containing ions, such as phosphate-buffered saline (PBS) and cell culture media, making them well-suited for use in long-term cell culture experiments. Besides their biocompatibility and low driving voltage, several examples illustrated the potential of IPMCs in modeling artificial muscles[169], in the form of mechanical stimulation of tissues[155], and enabling active microfluidic components such as micropumps[156,157]. Piezoelectric materials and IPMCs could conceivably be tailored to envelop tubular structures and thus induce mechanical motion: they could be integrated to generate physiologically relevant circumferential strain values in a vessel model and peristaltic movement in an intestine model, without needing external pressure sources and vacuum chambers. Although, at present, these materials exert less force than pneumatic alternatives, they hold great potential to simplify the geometry and fabrication of MPS by enabling electrically-activated movements in specified locations of the device (e.g. membranes, pillars).

One alternative for stimulation, optogenetics, requires genetic engineering of cells but can actuate muscle contraction very accurately. Local optogenetic stimulation of engineered light-sensitive tissues *in vitro* is enabled by the optical transparency of MPS, as demonstrated in a 3D model of 'Amyotrophic Lateral Sclerosis-on-Chip' where light was used to activate muscle contraction[158].

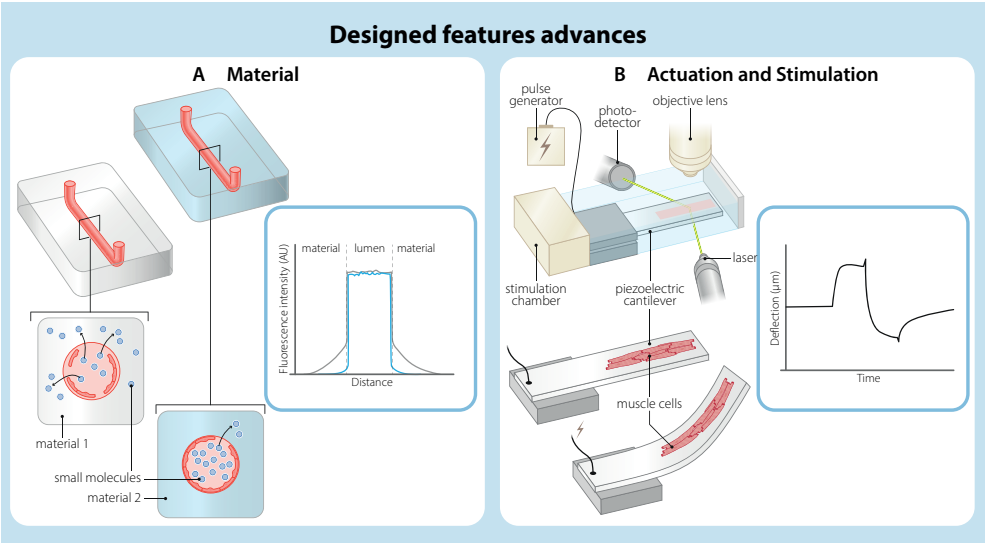

Figure 6: Technical advances that improve the quantification of designed and emergent physiological features in microphysiological systems.
Technical advances in materials and actuation or stimulation methods can improve the approximation of in vivo observations and quantitative control of designed features. A) Materials. Several features of structural materials can be tailored for MPS use. In particular, small molecule absorption by common elastomers such as PDMS can be overcome by using alternative polymers, as well as by implementing alternative elastomer formulations or targeted surface functionalizations, which enhance long-term hydrophilicity and may additionally favor cell adhesion. B) Actuation and stimulation. Local stimulation of tissues can be provided by means of mechanical structures made of electrically-responsive materials, such as piezoelectric materials and electro-active polymers. As an example, patterned piezoelectric cantilevers can bend upon electric input to provide controlled stretching to thin muscular films or cardiac tissues. Displacement of the cantilever can be tracked by optical means and correlated to induced tissue deformation. The inverse piezoelectric effect could in turn be exploited to detect inherent tissue motion. A) Based on REF.[119,149] B) Based on REF.[153]

Emergent features

There are multiple technical advances that could improve quantification or real-time monitoring of physiological features in MPS. They can be subdivided into electrical, electrochemical, optical and microwave sensing (*Figure 7*). As discussed previously, most current and commonly used MPS lack embedded sensing modalities, thereby limiting the number of physiological features that can be quantified. The techniques discussed here can be integrated into MPS as sensors, which enables higher sensitivity and reliability due to reduced distance between biological cue and sensor (*in situ* sensing), and provides real-time data that can yield direct feedback in an ongoing experiment. It should be noted that in most cases the sensing structures integrated into the MPS need to be coupled to external input and/or readout units, which may limit the portability of the MPS itself and the use of the MPS in conditioned environments, such as cell culture incubators. Design of external units

which are portable or compact enough to be combined with- and ultimately embedded in the MPS should be encouraged. The standardized interfacing of open platforms can provide improvements to this end, as described in *SI Note 7*.

Electrical, electrochemical, optical and microwave sensing options enable the quantification of similar physiological features with different techniques. As the integration of these sensing modalities within MPS is still in development and will be further optimized, it is still too early to quantitively compare and establish which technique is best suited for the measurement of which feature. In the future, quantification of features using different available sensing options will provide insight in this respect.

Electrical Sensing

One of the most widely used electrical sensing systems is TEER, commonly employed in systems modeling barrier tissues, such as VoCs, GoCs and Skin-on-Chips for quantitative barrier integrity assessment, as described earlier. TEER is usually based on applying voltage at DC or at a single and low frequency (e.g. 12.5 Hz or 75 Hz in common commercially available tools). By contrast, impedance spectroscopy (IS) uses voltage frequency sweeps to additionally quantify capacitive contributions to impedance in combination with equivalent electric circuit analysis[159]. IS can be useful to quantify TEER and other features, such as villus-like fold formation in GoCs[160] and development of epidermal multilayer structure in Skin-on-Chip[161]. While straightforward for quantification, barrier integrity measurements are prone to inconsistency and are difficult to standardize, making comparisons difficult. Specifically, non-uniform current density over the area of cell coverage, monitoring the whole cell layer rather than around the electrodes only, differences in temperature, system-to-system differences and measurement repeatability, and long-term electrode saturation remain challenges. One solution is to use correction factors for some of these parameters[162,163]. Importantly, sensitivity field calculations can help optimize electrode geometry and configuration to focus the measurement on the desired device volume[164]. Higher sensitivity can be obtained by specifically placing and multiplexing electrodes either on the side of the device culture area[165] or on membranes[166].

IS can be extended in a single MPS device by combination with additional multi-electrode arrays[167] and with sensors monitoring e.g. pH, oxygen content or specific biomarkers. The additional sensors may also be based on electric impedance measurement, as achieved through the functionalization of the electrode surface with selective chemistry[168]. IS can be further improved and adapted for 3D tissues and cell constructs by integrating electrodes within confining 3D geometries (e.g. microfluidic traps[169], pendant drops[170]) and in combination with 3D scaffolds[171]. Whereas most common scaffolds, made from gels or hydrogels, are electrically passive, use of electroactive polymeric scaffolds for IS with promising outcomes has also been reported. For instance, hollow tubular PEDOT:PSS structures can be used to grow intestinal epithelial cells for 26 days. The electrical properties

of the PEDOT:PSS scaffold promote better coupling of cells to electrode, and the position of the electrodes allows them to have dual sensing modalities: electrode-mode and transistor-mode. This allows monitoring of cell substrate coverage and sensing constriction in tubular structures, as in vascular reactivity[172].

Electrochemical sensing

Electrochemical sensors convert the effect of electrochemical interactions between analytes and electrodes into electrical signals. The surface of sensing electrodes can be functionalized by biomarkers tailored for selectivity and sensitivity[173]. Integrated within MPS, miniature affinity-based electrochemical sensors can be used for continuous monitoring of (secreted) biomarkers, providing real-time read-outs of biological responses and thus opportunities to correct and control fluctuations within an experiment[174]. Multiplexing of read-outs from multiple selective sensors or sensor electrodes can additionally enable high-throughput sensing of several biochemical markers[168]. This makes electrochemical sensors powerful alternatives to standard enzyme-linked immunosorbent assay (ELISA) protein measurements in culture medium and enables the quantification of multiple physiological features in OoC flow-through in real-time, such as secreted cytokines, (drug) metabolites and transport of compounds over a cell layer[175]. Recently, functionalized electrochemical sensors were integrated into a multi-OoC platform (liver-heart) to measure three different biomarkers (albumin, GST-α and CK-MB). The reported detection limit of albumin (0.1 ng/mL) showed superior range and sensitivity[176,177] compared to clinical tests on blood and urine in which the normal range is between 0.034-0.054 g/mL. This demonstrates that this type of readout is particularly suitable for quantitative comparison of different biomarkers and small analytes in MPS with clinical measurements of the same compounds in urine and blood.

The functionality of electrochemical sensors depends on the spatial distribution and position of electrodes within the MPS. The use of miniaturized electrochemical sensors that inherently amplify electric signals, represented by a class of field-effect transistors (FETs), allows integration of many sensors, increasing the spatial resolution of detection of analytes throughout the system[178].

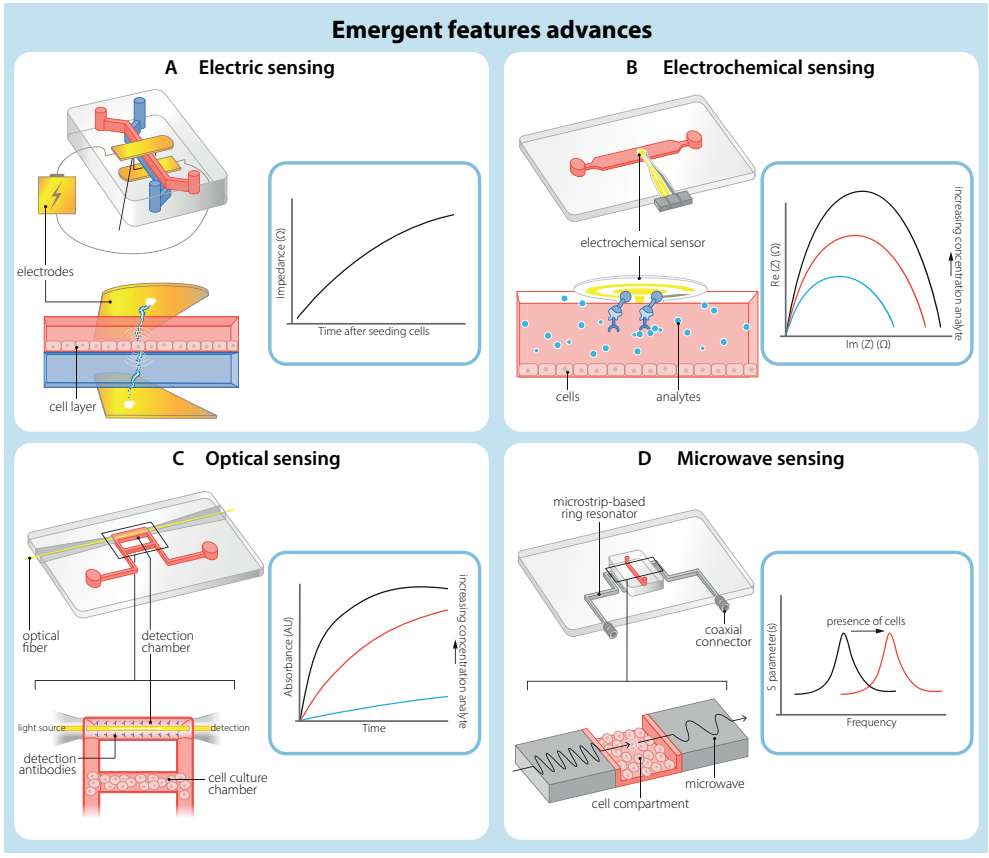

Figure 7: Technical advances that improve the quantification of emergent physiological features in microphysiological systems.

Technical advances in electrical sensing, electrochemical sensing, optical sensing and microwave sensing can yield advanced read-out systems that enable or improve quantification of emergent features. Most of these sensing solutions are based on electrodes and thin film technology originally developed for microelectronics, thus inheriting much available expertise and advantages in miniaturization, integrability and scalability. A) Electric sensing. Electric parameters of tissues, such as their resistance and capacitance (i.e. electric impedance), can be monitored continuously and correlated with their functionality (e.g. tightness of a tissue barrier, tissue composition). Measurements of trans-epithelial or -endothelial resistance and more generally impedance spectroscopy can be conducted by flanking tissues with pairs of electrodes and subjecting the tissues to electric fields of a range of frequencies. B) Electrochemical sensing. In electrochemical sensing, both amperometric and voltametric, surface chemical reactions can be exploited to trigger an electric output correlated to changes in the local microenvironment, as caused by e.g. tissue metabolism, medium composition. Selective surface functionalization of electrodes enables a high degree of selectivity and multiplexing. C) Optical sensing. Besides enabling optical inspection by microscopy, lightwaves are convenient sensing beacons, since parameters of lightwaves such as frequency, amplitude and their interference can be extremely sensitive to changes in the optical path, such as medium density and transparency. This makes integrating optical waveguiding structures such as optical fibers appealing for MPS applications. D) Microwave sensing. Microwaves occupy a specific portion of the electromagnetic spectrum, and can be injected and confined within microengineered structures, such as ring oscillators based on microstrip lines.

They are thereby uesful as sensitive detectors of local changes in permittivity induced by e.g. cells or medium composition. A) Based on REF.[160] B) Based on REF.[179] C) Based on REF.[176] D) Based on REF. [180]

Optical Sensing

Optical sensors commonly detect changes in optical or geometrical properties (e.g. color, luminescence, absorption, scattering, refractive index, size and shape depending on geometric boundaries) of media and of their local environment by measuring changes in the properties of optical waves (amplitude, wavelength, phase) used as probes. In MPS, the changes can be caused by a variety of factors, such as tissue metabolism and dynamics, and media composition including analytes of interest and optical reporters[181].

Optical sensors can monitor small biological cues such as cytokines, providing opportunities to standardize MPS platforms. In one example, microfluidics was integrated with an optical fiber-based sensing unit measuring optical absorbance to quantify IL-2 secreted by lymphocytes. This photonic Lab-on-Chip (Ph-LoC) provides an alternative to an ELISA. IL-2 concentrations ranging from 50 to 1000 pg/mL could be measured in just 30 minutes. The range and application of this Ph-LoC depends on antibody availability but is already suitable for monitoring of most common cytokines[179.] It is also possible to multiplex this platform and simultaneously quantify different cytokines using an array of silicon photonic micro ring resonators. The shifts in resonance wavelength upon binding of the target molecule to the ring surface distinguishes the different cytokines, without needing specific labeling and enabling continuous measurements, opposite to currently used techniques[182].

Quantification of many physiological features in MPS, such as the tissue architecture, cell morphology, mucus layer thickness, cell surface area and fluid flow rate, often relies on imaging technologies able to penetrate tissues and substrate materials while maintaining good resolution. Optical coherence tomography (OCT) provides an imaging method that allows real-time 3D imaging of (relatively large) structures in MPS without using immunostaining or fluorescent reporter lines[183]. The technique is based on measuring the interference between a reference light beam and backscattered light to reconstruct the profile of the sample under consideration; the imaging depth can reach to more than 1 mm[184]; however resolution is somewhat lower than conventional microscopy (~6 µm versus < 1 µm, respectively)[185]. This imaging technique enables in particular continuous monitoring and quantification of 3D (luminal) structures in MPS and was used to study sprouting angiogenesis in a VoC model and engineered microvessels in a MPS of the outer blood-retinal barrier[185,186].

Microwave Sensing

Similar to electric impedance and optical sensing, electromagnetic waves in the microwave range (~1-40 GHz) can be used for contactless sensing as well. In this case, the sensing

principle is based on measuring how the electromagnetic waves interact with and penetrate into materials. Penetration depends on frequency and the electrical characteristics of the material, mainly the permittivity. Electromagnetic waves at microwave frequencies can penetrate the cell, while leaving it intact[187], and reveal information about the intracellular composition[188]. This biosensing alternative allows label-free, non-intrusive, real-time discrimination, localization and counting of cells[189], and can specifically be useful to quantify cell type ratios at any given time in MPS.

A microwave sensor based on impedance spectroscopy was proposed which could determine cell diversity at the single-cell level, demonstrating label-free cell identification at microwave frequencies[187]. A real-time and flow-through sensor was developed within an integrated multi-mode microwave resonator which was able to distinguish two different cancer cell lines, HeLa and MDA-MB-157, in mixed populations[190]. In the future, integration of real-time microwave sensors could improve quantification of different cell types within a culture platform and reveal spatial information of individual cells within a 3D tissue. This real-time information on the numbers and ratios of different cell types in MPS will facilitate standardized quantification of other physiological features that depend on normalization to the number of a specific cell type.

Additionally, microwave supporting structures such as resonators and microstrip lines can be embedded into microfluidic systems as part of highly sensitive sensors for flow rates and fluid composition with an electric readout. Split ring microwave resonators coupled to an interferometric system were used for high-sensitivity measurement of glucose concentration in a microfluidic setup[191]. A fluid flow sensor embedded in a microfluidic device exploited the flow rate-dependent deformation of a thin circular membrane integrated within a planar microwave ring resonator, and the subsequent alteration of the effective permittivity of the surrounding medium, to measure flow rates in the range of 0.5 to 300 µL/min with a resolution of 1 µL/min[192]. These and similar systems are supported by accurate analytical and numerical models to predict and quantify sensor performance, and by electronic readout systems which could be integrated into compact electric layers (e.g. printed circuit boards) connected to the sensing structures.

Conclusion and Outlook

MPS are clearly poised to contribute to biomedical research, but in order to take the technology to the next level and realize end-user and regulatory acceptance, it is essential to understand their predictive value. With the growing number of users in this relatively new field, it is widely accepted that consensus on qualification and standardization methods for MPS technology is urgent to realize their full potential. Quantification of physiological features in design and read-outs of MPS leads the way towards establishing accurate comparisons between different *in vitro* models and *in vivo* (human) physiology, contributing to development of measurable standards to qualify MPS as fit-for-purpose in application.

The comprehensive overview of quantified physiological features of healthy organ function in MPS, as provided in this review, serves as a resource for the development of these measurable standards and can be used as basis for the quantification of disease phenotypes and drug efficacy and toxicity, which are defined by deviations in the same physiological features. These type of quantifications will be key to uncover the predictive value of MPS and accelerate the implementation of MPS in the drug development pipeline.

MPS are specifically suitable for providing quantitative approximations of diverse physiological features as they allow versatile designs and integration of sensors and read-out methods. Categorizing the desired quantifiable physiological features in designed (directly translatable in device design or input) and emergent features (emerging cellular function) will facilitate quantification in MPS, as both types of features require different strategies. For quantifying designed features, it is essential to consider the relevant technology or material needed to incorporate a specific feature in MPS design in the desired range. Quantification of emergent features requires incorporation of the relevant sensing and read-out system to accurately monitor cellular responses using standardized methods and units. To further steer the exact value of an emergent feature, which might be required to qualify the system fit-for-purpose, the designed features that influence the emergent feature need to be determined and adapted. The examples and considerations highlighted in this review will allow users to select the relevant design options and sensing technologies to optimize quantification of the designed and emergent features of interest. These examples demonstrate that current work already allows direct comparison of data from MPS with *in vivo* measures, however, they also reveal room for improvement. Current limitations in quantitative comparisons of physiological features in MPS with *in vivo* observations include differences in scale, methods of quantification, resolution and duration.

While MPS generally try to mimic *in vivo* tissue architecture, their main goal is to recapitulate one or multiple functional features of an organ, depending on the research question of interest. As such, they do not necessarily have to recapitulate the exact dimensions of the human body. When functional features are investigated which are influenced by the dimensions of the tissue, scaling and normalization becomes a necessity. To compare *in vitro* MPS with *in vivo* measurements, it is essential to correct for differences in surface-to-volume and cell-to-volume ratios[193]. In some cases, it might be sufficient simply to normalize to liquid volume, number of cells and dimensions (e.g. when converting absolute fluid flow rate to WSS); however, for more complex features and systems there will be new opportunities to integrate *in silico* modeling to address this issue, as done previously for a multi-organ platform[194].

When the quantification method of a specific physiological feature differs between systems, it becomes more difficult to compare data accurately. Specifically, for emergent features that describe complex cellular functions, many different quantification methods and units are used. More clarity is needed on how data is measured and reported in clinical

settings and whether it is feasible to replicate this in model systems. For certain features, this is more straightforward e.g. measurement of secreted products in circulation and flow through, than for others e.g. barrier integrity measurement. For physiological features that are not amenable to such a direct translation of measurement method, the field should reach consensus on how to quantify and report the data in a standardized way. This review has outlined a basis for the standardization of quantification methods and data reporting for some important physiological features.

Some of these features are location- and time-dependent and can be quantified in high resolution in MPS but not *in vivo* (e.g. cytokine secretion). For these features it is currently difficult to have a direct comparison between MPS and *in vivo* data. One solution is focusing on the relative changes in cellular function induced by clinically tested reference compounds. These will be valuable benchmark measures for drug development and useful for the uptake of MPS technology by regulatory authorities and pharmaceutical companies. In the future, coupling multi organ-chips might allow modelling of local and systemic responses.

MPS are designed at present to mimic and monitor aspects of tissue (patho) physiology over relatively short periods of days or weeks. Drug responses and clearance by tissues in the MPS are likewise acute, but chronic effects of drugs for example cannot be monitored since long-term culture of cells in the devices has only been realised in a limited number of cases. Achieving this will require at a minimum next-generation devices, materials, pumps and sensors as well as culture media that are better mimics of body fluids. It may then be possible to couple multiple MPS devices in series or parallel to mimic organ and tissue interactions in the human body as never before.

Finally, the next level of MPS will require greater precision in exactly what is being captured by sophisticated sensors and systems: are the responses typical of fetal, adult or even aged tissue and organs? Are pathological responses correctable by therapeutic approaches, and is the timing of such interventions relevant when compared to the actual progression of disease? If we are to develop MPS models that address such questions, this will critically depend on the quantitative approach outlined in the review. The concept of quantitatively measuring designed and emergent physiological features represents an important first step towards creating a database that is publicly-available and will facilitate the benchmarking of a diverse range of MPS to other MPS and to (human) *in vivo* data. One approach would be to create an open access MPS “atlas” much like the Human Cell Atlas. The adapted mission statement could be similar: to create comprehensive references of all human MPS as a basis for both understanding human health and diagnosing, monitoring, and treating disease. Such an atlas could contain the available quantifications of designed and emergent physiological features of a wide range of MPS and, besides functioning as reference dataset, provide insight into which designed features are important to implement in an MPS to steer an emergent feature of interest.

In conclusion, all considerations described are of importance to achieve proper quantification, standardization and extrapolation of *in vitro* to *in vivo* data improvements. Notably, with the many technical options available to design MPS and integrate sensors and read-outs, it becomes increasingly important to report the rationale of certain design choices and how they relate to the physiology that is recapitulated. In addition, by reporting the quantitative output of MPS in a comparable and translatable way, transparency is created in the potency of these models to accurately predict and replicate specific physiological processes. More emphasis and discussion on the quantification of physiological features in MPS, as opposed to qualitative implementation, will be essential to define measurable standards for model qualification and standardization in a time of rapidly increasing numbers of MPS designs and users.

Acknowledgements

This work was supported by the Netherlands Organ-on-Chip Initiative, an NWO Gravitation project (024.003.001) funded by the Ministry of Education, Culture, and Science of the government of The Netherlands. We thank A. van den Berg, H. Clevers, P.M. Sarro, M.D. Ferrari, C. Wijmenga, S.A. Kushner, A.M.J.M. van den Maagdenberg and J. Gribnau for their leadership in the Netherlands Organ-on-Chip Initiative, constructive discussions and creating the collaborative environment on which this review was based. We thank Manon Zuurmond for her work as graphical designer on the figures. Some components of the figures were created using Biorender.com.

References

1. Ingber, D. E. Human organs-on-chips for disease modelling, drug development and personalized medicine. *Nat. Rev. Genet.* (2022) doi:10.1038/s41576-022-00466-9.
2. Vunjak-Novakovic, G., Ronaldson-Bouchard, K. & Radisic, M. Organs-on-a-chip models for biological research. *Cell* **184**, 4597–4611 (2021).
3. Mastrangeli, M., Millet, S. & van den Eijnden-Van Raaij, J. Organ-on-chip in development: Towards a roadmap for organs-on-chip. *ALTEX* **36**, 650–668 (2019).
4. Ingber, D. E. Reverse Engineering Human Pathophysiology with Organs-on-Chips. *Cell* **164**, 1105–1109 (2016).
5. Low, L. A., Mummery, C. L., Berridge, B. R., Austin, C. P. & Tagle, D. A. Organs-on-chips: into the next decade. *Nat. Rev. Drug Discov.* (2020) doi:10.1038/s41573-020-0079-3.
6. Mastrangeli, M. *et al.* Building blocks for a European organ-on-chip roadmap. *ALTEX* **36**, 481–492 (2019).
7. Qiu, Y. *et al.* Microvasculature-on-a-chip for the long-term study of endothelial barrier dysfunction and microvascular obstruction in disease. *Nat Biomed Eng* **2**, 453–463 (2018).
8. Park, T.-E. *et al.* Hypoxia-enhanced Blood-Brain Barrier Chip recapitulates human barrier function, drug penetration, and antibody shuttling properties. *Nat. Commun.* 482463 (2019) doi:10.1101/482463.
9. Van Duinen, V. *et al.* 96 Perfusable Blood Vessels To Study Vascular Permeability in Vitro. *Sci. Rep.* **7**, 1–11 (2017).
10. de Graaf, M. N. S. *et al.* Scalable microphysiological system to model three-dimensional blood vessels. *APL Bioeng.* **3**, 026105 (2019).
11. Linville, R. M. *et al.* Human iPSC-derived blood-brain barrier microvessels: validation of barrier function and endothelial cell behavior. *Biomaterials* **190**–**191**, 24–37 (2019).
12. Brandenberg, N. & Lutolf, M. P. In Situ Patterning of Microfluidic Networks in 3D Cell-Laden Hydrogels. *Adv. Mater.* **28**, 7450–7456 (2016).
13. Enrico, A. *et al.* Three Dimensional Microvascularized Tissue Models by Laser-Based Cavitation Molding of Collagen. *Adv. Mater.* **34**, (2022).
14. Kim, S., Lee, H., Chung, M. & Jeon, N. L. Engineering of functional, perfusable 3D microvascular networks on a chip. *Lab Chip* **13**, 1489–1500 (2013).
15. Campisi, M. *et al.* 3D self-organized microvascular model of the human blood-brain barrier with endothelial cells, pericytes and astrocytes. *Biomaterials* **180**, 117–129 (2018).
16. Vila Cuenca, M. *et al.* Engineered 3D vessel-on-chip using hiPSC-derived endothelial- and vascular smooth muscle cells. *Stem Cell Reports* **16**, (2021).
17. Wu, Z. *et al.* Microfluidic Printing of Tunable Hollow Microfibers for Vascular Tissue Engineering. *Adv. Mater. Technol.* **6**, (2021).
18. Gao, W. *et al.* One-Step Formation of Protein-Based Tubular Structures for Functional Devices and Tissues. *Adv. Healthc. Mater.* **10**, (2021).
19. Kim, H., Huh, D., Hamilton, G. & Ingber, D. Human gut-on-a-chip inhabited by microbial flora that experiences intestinal peristalsis-like motions and flow. *Lab Chip* **12**, 2165–2174 (2012).
20. Shin, Y. C. *et al.* Three-dimensional regeneration of patient-derived intestinal organoid epithelium in a physiodynamic mucosal interface-on-a-chip. *Micromachines* **11**, 663 (2020).
21. Naumovska, E. *et al.* Direct on-chip differentiation of intestinal tubules from induced pluripotent stem cells. *Int. J. Mol. Sci.* **21**, (2020).
22. Beaurivage, C. *et al.* Development of a human primary gut-on-a-chip to model inflammatory processes. *Sci. Rep.* **10**, (2020).
23. Pocock, K. *et al.* Intestine-on-A-Chip Microfluidic Model for Efficient in Vitro Screening of Oral Chemotherapeutic Uptake. *ACS Biomater. Sci. Eng.* **3**, 951–959 (2017).
24. Nikolaev, M. *et al.* Homeostatic mini-intestines through scaffold-guided organoid morphogenesis. *Nature* **585**, 574–578 (2020).
25. Shim, K. Y. *et al.* Microfluidic gut-on-a-chip with three-dimensional villi structure. *Biomed. Microdevices* **19**, (2017).
26. Mills, R. J. *et al.* Functional screening in human cardiac organoids reveals a metabolic mechanism for cardiomyocyte cell cycle arrest. *Proc. Natl. Acad. Sci.* **114**, E8372–E8381 (2017).
27. Dostanić, M. *et al.* A Miniaturized EHT Platform for Accurate Measurements of Tissue Contractile

Properties. *J. Microelectromechanical Syst.* **29**, 881–887 (2020).
28. Mannhardt, I. *et al.* Comparison of 10 Control hPSC Lines for Drug Screening in an Engineered Heart Tissue Format. *Stem Cell Reports* **15**, 983–998 (2020).
29. Zhao, Y. *et al.* A Platform for Generation of Chamber-Specific Cardiac Tissues and Disease Modeling. *Cell* **176**, 913–927 (2019).
30. Vivas, A. *et al.* Generation and Culture of Cardiac Microtissues in a Microfluidic Chip with a Reversible Open Top Enables Electrical Pacing, Dynamic Drug Dosing and Endothelial Cell Co-Culture. *Adv. Mater. Technol.* **7**, (2022).
31. Mathur, A. *et al.* Human iPSC-based cardiac microphysiological system for drug screening applications. *Sci. Rep.* **5**, 8883 (2015).
32. MacQueen, L. A. *et al.* A tissue-engineered scale model of the heart ventricle. *Nat. Biomed. Eng.* **2**, 930–941 (2018).
33. Sarkar, A. *et al.* Efficient Generation of CA3 Neurons from Human Pluripotent Stem Cells Enables Modeling of Hippocampal Connectivity In Vitro. *Cell Stem Cell* **22**, 684–697 (2018).
34. Odawara, A., Gotoh, M. & Suzuki, I. A three-dimensional neuronal culture technique that controls the direction of neurite elongation and the position of soma to mimic the layered structure of the brain. *RSC Adv.* **3**, 23620–23630 (2013).
35. Dauth, S. *et al.* Neurons derived from different brain regions are inherently different in vitro: A novel multiregional brain-on-a-chip. *J. Neurophysiol.* **117**, 1320–1341 (2017).
36. Rifes, P. *et al.* Modeling neural tube development by differentiation of human embryonic stem cells in a microfluidic WNT gradient. *Nat. Biotechnol.* **38**, 1265–1273 (2020).
37. Nordström, U., Jessell, T. M. & Edlund, T. Progressive induction of caudal neural character by graded Wnt signaling. *Nat. Neurosci.* **5**, 525–532 (2002).
38. Trujillo, C. A. *et al.* Complex Oscillatory Waves Emerging from Cortical Organoids Model Early Human Brain Network Development. *Cell Stem Cell* **25**, 558–569 (2019).
39. Brandenberg, N. & Lutolf, M. P. In Situ Patterning of Microfluidic Networks in 3D Cell-Laden Hydrogels. *Adv. Mater.* **28**, 7450–7456 (2016).
40. Pollet, A. M. A. O. & den Toonder, J. M. J. Recapitulating the vasculature using Organ-on-Chip technology. *Bioengineering* **7**, 1–18 (2020).
41. Helander, H. F. & Fändriks, L. Surface area of the digestive tract-revisited. *Scand. J. Gastroenterol.* **49**, 681–689 (2014).
42. Hasan, M. & Ferguson, A. Measurements of intestinal villi in non-specific and ulcer-associated duodenitis - correlation between area of microdissected villus and villus epithelial cell count. *J. Clin. Pathol.* **34**, 1181–1186 (1981).
43. Marsh, M. N. & Swift, J. A. A study of the small intestinal mucosa using the scanning electron microscope. *Gut* **10**, 940–949 (1969).
44. Trbojević-Stanković, J. B. *et al.* Morphometric study of healthy jejunal and ileal mucosa in adult and aged subjects. *Histol Histopathol* **25**, 153–158 (2010).
45. Lin, F. Y. *et al.* Cardiac Chamber Volumes, Function, and Mass as Determined by 64-Multidetector Row Computed Tomography. *JACC Cardiovasc. Imaging* **1**, 782–786 (2008).
46. Adler, D. H. *et al.* Characterizing the human hippocampus in aging and Alzheimer's disease using a computational atlas derived from ex vivo MRI and histology. *Proc. Natl. Acad. Sci. U. S. A.* **115**, 4252–4257 (2018).
47. Nowakowski, T. J., Pollen, A. A., Sandoval-Espinosa, C. & Kriegstein, A. R. Transformation of the Radial Glia Scaffold Demarcates Two Stages of Human Cerebral Cortex Development. *Neuron* **91**, 1219–1227 (2016).
48. Song, J. W. *et al.* Computer-controlled microcirculatory support system for endothelial cell culture and shearing. *Anal. Chem.* **77**, 3993–3999 (2005).
49. Arora, S., Lam, A. J. Y., Cheung, C., Yim, E. K. F. & Toh, Y. C. Determination of critical shear stress for maturation of human pluripotent stem cell-derived endothelial cells towards an arterial subtype. *Biotechnol. Bioeng.* **116**, 1164–1175 (2019).
50. Chen, H. *et al.* Cardiac-like flow generator for long-term imaging of endothelial cell responses to circulatory pulsatile flow at microscale. *Lab Chip* **13**, 2999–3007 (2013).
51. Satoh, T. *et al.* A pneumatic pressure-driven multi-throughput microfluidic circulation culture system. *Lab Chip* **16**, 2339–2348 (2016).

52. Popel, A. S. & Johnson, P. C. Microcirculation and hemorheology. *Annual Review of Fluid Mechanics* vol. 37 43–69 (2005).
53. Callaghan, F. M. & Grieve, S. M. Normal patterns of thoracic aortic wall shear stress measured using four-dimensional flow MRI in a large population. *Am. J. Physiol. - Hear. Circ. Physiol.* **315**, H1174–H1181 (2018).
54. Dessalles, C. A., Ramón-Lozano, C., Babataheri, A. & Barakat, A. I. Luminal flow actuation generates coupled shear and strain in a microvessel-on-chip. *Biofabrication* **14**, (2021).
55. Dobrin, P. B. Mechanical properties of arteries. *Physiol. Rev.* **58**, (1978).
56. Morrison, T. M., Choi, G., Zarins, C. K. & Taylor, C. A. Circumferential and longitudinal cyclic strain of the human thoracic aorta: Age-related changes. *J. Vasc. Surg.* **49**, 1029–1036 (2009).
57. Wasson, E. M., Dubbin, K. & Moya, M. L. Go with the flow: modeling unique biological flows in engineered in vitro platforms. *Lab Chip* **21**, 2095–2120 (2021).
58. Dutton, J. S., Hinman, S. S., Kim, R., Wang, Y. & Allbritton, N. L. Primary Cell-Derived Intestinal Models: Recapitulating Physiology. *Trends Biotechnol.* **37**, 744–760 (2019).
59. Park, J. *et al.* Three-dimensional brain-on-a-chip with an interstitial level of flow and its application as an in vitro model of Alzheimer's disease. *Lab Chip* **15**, 141–150 (2015).
60. Lindstrøm, E. K., Ringstad, G., Mardal, K. A. & Eide, P. K. Cerebrospinal fluid volumetric net flow rate and direction in idiopathic normal pressure hydrocephalus. *NeuroImage Clin.* **20**, 731–741 (2018).
61. Basson, M. D. Paradigms for Mechanical Signal Transduction in the Intestinal Epithelium. *Digestion* **68**, 217–225 (2003).
62. Rodriguez, M. L., Werner, T. R., Becker, B., Eschenhagen, T. & Hirt, M. N. Magnetics-Based Approach for Fine-Tuning Afterload in Engineered Heart Tissues. *ACS Biomater. Sci. Eng.* **5**, 3663–3675 (2019).
63. Trappmann, B. *et al.* Matrix degradability controls multicellularity of 3D cell migration. *Nat. Commun.* **8**, (2017).
64. Gordon, E., Schimmel, L. & Frye, M. The Importance of Mechanical Forces for in vitro Endothelial Cell Biology. *Front. Physiol.* **11**, (2020).
65. Onfroy-Roy, L., Hamel, D., Foncy, J., Malaquin, L. & Ferrand, A. Extracellular Matrix Mechanical Properties and Regulation of the Intestinal Stem Cells: When Mechanics Control Fate. *Cells* **9**, 1–23 (2020).
66. Wang, Y. *et al.* A microengineered collagen scaffold for generating a polarized crypt-villus architecture of human small intestinal epithelium. *Biomaterials* **128**, 44–55 (2017).
67. Pasqualini, F. S. *et al.* Traction force microscopy of engineered cardiac tissues. *PLoS One* **13**, 1–14 (2018).
68. McCain, M. L., Yuan, H., Pasqualini, F. S., Campbell, P. H. & Parker, K. K. Matrix elasticity regulates the optimal cardiac myocyte shape for contractility. *Am. J. Physiol. - Hear. Circ. Physiol.* **306**, 1525–1539 (2014).
69. Cho, A. N. *et al.* Microfluidic device with brain extracellular matrix promotes structural and functional maturation of human brain organoids. *Nat. Commun.* **12**, (2021).
70. Barnes, J. M., Przybyla, L. & Weaver, V. M. Tissue mechanics regulate brain development, homeostasis and disease. *J. Cell Sci.* **130**, 71–82 (2017).
71. Lam, S. F., Shirure, V. S., Chu, Y. E., Soetikno, A. G. & George, S. C. Microfluidic device to attain high spatial and temporal control of oxygen. *PLoS One* **13**, 1–16 (2018).
72. Carreau, A., Hafny-Rahbi, B. El, Matejuk, A., Grillon, C. & Kieda, C. Why is the partial oxygen pressure of human tissues a crucial parameter? Small molecules and hypoxia. *J. Cell. Mol. Med.* **15**, 1239–1253 (2011).
73. Jalili-firoozinezhad, S. *et al.* A complex human gut microbiome cultured in an anaerobic intestine-on-a-chip. *Nat. Biomed. Eng.* **3**, 520–531 (2019).
74. Ast, T. & Mootha, V. K. Oxygen and mammalian cell culture: are we repeating the experiment of Dr. Ox? *Nat. Metab.* **1**, 858–860 (2019).
75. Veldhuizen, J. *et al.* Cardiac ischemia on-a-chip to investigate cellular and molecular response of myocardial tissue under hypoxia. *Biomaterials* **281**, (2022).
76. Winegrad, S., Henrion, D., Rappaport, L. & Samuel, J. L. Self-protection by cardiac myocytes against hypoxia and hyperoxia. *Circ. Res.* **85**, 690–698 (1999).
77. Erecińska, M. & Silver, I. A. Tissue oxygen tension and brain sensitivity to hypoxia. *Respir. Physiol.* **128**, 263–276 (2001).
78. Winkler, E. A. *et al.* A single-cell atlas of the normal and malformed human brain vasculature. *Science*

(80-.). **7377**, 1–23 (2022).
79. Wang, Y. *et al.* Single-cell transcriptome analysis reveals differential nutrient absorption functions in human intestine. *J. Exp. Med.* **217**, (2019).
80. Tucker, N. R. *et al.* Transcriptional and Cellular Diversity of the Human Heart. *Circulation* **142**, 466–482 (2020).
81. Litviňuková, M. *et al.* Cells of the adult human heart. *Nature* **588**, 466–472 (2020).
82. Miterko, L. N., Lackey, E. P., Heck, D. H. & Sillitoe, R. V. Shaping Diversity Into the Brain's Form and Function. *Frontiers in Neural Circuits* vol. 12 83 (2018).
83. Bhaduri, A. *et al.* An atlas of cortical arealization identifies dynamic molecular signatures. *Nature* **598**, 200–204 (2021).
84. Winkelman, M. A. *et al.* Interstitial flow enhances the formation, connectivity, and function of 3D brain microvascular networks generated within a microfluidic device. *Lab Chip* **22**, 170–192 (2022).
85. Mathiisen, T. M., Lehre, K. P., Danbolt, N. C. & Ottersen, O. P. The perivascular astroglial sheath provides a complete covering of the brain microvessels: An electron microscopic 3D reconstruction. *Glia* **58**, 1094–1103 (2010).
86. Armulik, A., Genové, G. & Betsholtz, C. Pericytes: Developmental, Physiological, and Pathological Perspectives, Problems, and Promises. *Dev. Cell* **21**, 193–215 (2011).
87. Hinman, S. S., Wang, Y. & Allbritton, N. L. Photopatterned Membranes and Chemical Gradients Enable Scalable Phenotypic Organization of Primary Human Colon Epithelial Models. *Anal. Chem.* **91**, 15240–15247 (2019).
88. Elmentaite, R. *et al.* Single-Cell Sequencing of Developing Human Gut Reveals Transcriptional Links to Childhood Crohn's Disease. *Dev. Cell* **55**, 771–783 (2020).
89. Wang, Y. F., Liu, C. & Xu, P. F. Deciphering and reconstitution of positional information in the human brain development. *Cell Regen.* **10**, 1–13 (2021).
90. Iannielli, A. *et al.* Reconstitution of the Human Nigro-striatal Pathway on-a-Chip Reveals OPA1-Dependent Mitochondrial Defects and Loss of Dopaminergic Synapses. *Cell Rep.* **29**, 4646–4656 (2019).
91. Alonso-Nanclares, L., Gonzalez-Soriano, J., Rodriguez, J. R. & DeFelipe, J. Gender differences in human cortical synaptic density. *Proc. Natl. Acad. Sci. U. S. A.* **105**, 14615–14619 (2008).
92. Yu, Y. *et al.* A microfluidic platform for continuous monitoring of dopamine homeostasis in dopaminergic cells. *Microsystems Nanoeng.* **5**, (2019).
93. Gonon, F. Prolonged and extrasynaptic excitatory action of dopamine mediated by D1 receptors in the rat striatum in vivo. *J. Neurosci.* **17**, 5972–5978 (1997).
94. Ford, C. P., Phillips, P. E. M. & Williams, J. T. The time course of dopamine transmission in the ventral tegmental area. *J. Neurosci.* **29**, 13344–13352 (2009).
95. Herland, A. *et al.* Distinct contributions of astrocytes and pericytes to neuroinflammation identified in a 3D human blood-brain barrier on a chip. *PLoS One* **11**, (2016).
96. Calandra, T., Gerain, J., Heumann, D., Baumgartner, J. D. & Glauser, M. P. High circulating levels of interleukin-6 in patients with septic shock: Evolution during sepsis, prognostic value, and interplay with other cytokines. *Am. J. Med.* **91**, 23–29 (1991).
97. Park, J. *et al.* A 3D human triculture system modeling neurodegeneration and neuroinflammation in Alzheimer's disease. *Nat. Neurosci.* **21**, 941–951 (2018).
98. Leng, F. & Edison, P. Neuroinflammation and microglial activation in Alzheimer disease: where do we go from here? *Nat. Rev. Neurol.* **17**, 157–172 (2021).
99. Yuan, W., Lv, Y., Zeng, M. & Fu, B. M. Non-invasive measurement of solute permeability in cerebral microvessels of the rat. *Microvasc. Res.* **77**, 166–173 (2009).
100. Nejdfors, P., Ekelund, M., Jeppsson, B. & Weström, B. R. Mucosal in vitro permeability in the intestinal tract of the pig, the rat, and man: Species- and region-related differences. *Scand. J. Gastroenterol.* **35**, 501–507 (2000).
101. Nunes, S. S. *et al.* Biowire: A platform for maturation of human pluripotent stem cell-derived cardiomyocytes. *Nat. Methods* **10**, 781–787 (2013).
102. Zhao, Y. *et al.* Towards chamber specific heart-on-a-chip for drug testing applications. *Adv. Drug Deliv. Rev.* **165**–**166**, 60–76 (2020).
103. Tiburcy, M. *et al.* Defined engineered human myocardium with advanced maturation for applications in heart failure modeling and repair. *Circulation* **135**, 1832–1847 (2017).
104. Thavandiran, N. *et al.* Design and formulation of functional pluripotent stem cell-derived cardiac

microtissues. *Proc. Natl. Acad. Sci.* **110**, E4698–E4707 (2013).
105. Gyorgy, B. & Andreas, D. Neuronal Oscillations in Cortical Networks. *Science (80-.).* **304**, 1926–1929 (2004).
106. Kim, S., Chung, M. & Jeon, N. L. Three-dimensional biomimetic model to reconstitute sprouting lymphangiogenesis in vitro. *Biomaterials* **78**, 115–128 (2016).
107. Darwich, A. S., Aslam, U., Ashcroft, D. M. & Rostami-Hodjegan, A. Meta-analysis of the turnover of intestinal epithelia in preclinical animal species and humans. *Drug Metab. Dispos.* **42**, 2016–2022 (2014).
108. Moutairou, K. *et al.* Epithelial cell migration on small intestinal villi in the neonatal rat. Comparison between [3H] thymidine and cytoplasmic labelling after Pu-citrate ingestion. *Biol. Cell* **65**, 265–269 (1989).
109. Parker, A. *et al.* Cell proliferation within small intestinal crypts is the principal driving force for cell migration on villi. *FASEB J.* **31**, 636–649 (2017).
110. Linville, R. M. *et al.* Human iPSC-derived blood-brain barrier microvessels: validation of barrier function and endothelial cell behavior. *Biomaterials* **190**–**191**, 24–37 (2019).
111. Chen, Y. *et al.* A microfluidic circulatory system integrated with capillary-assisted pressure sensors. *Lab Chip* **17**, 653–662 (2017).
112. Wasson, E. M., Dubbin, K. & Moya, M. L. Go with the flow: modeling unique biological flows in engineered in vitro platforms. *Lab Chip* **21**, 2095–2120 (2021).
113. Parsa, H., Wang, B. Z. & Vunjak-Novakovic, G. A microfluidic platform for the high-throughput study of pathological cardiac hypertrophy. *Lab Chip* **17**, 3264–3271 (2017).
114. Schroer, A., Pardon, G., Castillo, E., Blair, C. & Pruitt, B. Engineering hiPSC cardiomyocyte in vitro model systems for functional and structural assessment. *Prog. Biophys. Mol. Biol.* **144**, 3–15 (2019).
115. Mason, B. N., Starchenko, A., Williams, R. M., Bonassar, L. J. & Reinhart-King, C. A. Tuning three-dimensional collagen matrix stiffness independently of collagen concentration modulates endothelial cell behavior. *Acta Biomater.* **9**, 4635–4644 (2013).
116. Soofi, S. S., Last, J. A., Liliensiek, S. J., Nealey, P. F. & Murphy, C. J. Elastic modulus of Matrigel as determined by AFM. *J. Struct. Biol.* **167**, 216–219 (2009).
117. Fuard, D., Tzvetkova-Chevolleau, T., Decossas, S., Tracqui, P. & Schiavone, P. Optimization of poly-di-methyl-siloxane (PDMS) substrates for studying cellular adhesion and motility. *Microelectron. Eng.* **85**, 1289–1293 (2008).
118. Roy, E., Galas, J.-C. & Veres, T. Thermoplastic elastomers for microfluidics: Towards a high-throughput fabrication method of multilayered microfluidic devices. *Lab Chip* **11**, 3193 (2011).
119. Carlborg, C. F., Haraldsson, T., Öberg, K., Malkoch, M. & van der Wijngaart, W. Beyond PDMS: off-stoichiometry thiol–ene (OSTE) based soft lithography for rapid prototyping of microfluidic devices. *Lab Chip* **11**, 3136 (2011).
120. Radisic, M. & Loskill, P. Beyond PDMS and Membranes: New Materials for Organ-on-a-Chip Devices. *ACS Biomater. Sci. Eng.* **7**, 2861–2863 (2021).
121. Buguin, A., Li, M. H., Silberzan, P., Ladoux, B. & Keller, P. Micro-actuators: When artificial muscles made of nematic liquid crystal elastomers meet soft lithography. *J. Am. Chem. Soc.* **128**, 1088–1089 (2006).
122. Guin, T. *et al.* Layered liquid crystal elastomer actuators. *Nat. Commun.* **9**, 2531 (2018).
123. Chen, M. B., Srigunapalan, S., Wheeler, A. R. & Simmons, C. A. A 3D microfluidic platform incorporating methacrylated gelatin hydrogels to study physiological cardiovascular cell-cell interactions. *Lab Chip* **13**, 2591–2598 (2013).
124. Vickovic, S. *et al.* High-definition spatial transcriptomics for in situ tissue profiling. *Nat. Methods* **16**, 987–990 (2019).
125. Srivatsan, S. R. *et al.* Embryo-scale, single-cell spatial transcriptomics. *Science (80-.).* **373**, 111–117 (2021).
126. Fajgenbaum, D. C. & June, C. H. Cytokine Storm. *N. Engl. J. Med.* **383**, 2255–2273 (2020).
127. Hajal, C. *et al.* Engineered human blood–brain barrier microfluidic model for vascular permeability analyses. *Nat. Protoc.* **17**, 95–128 (2022).
128. Hajal, C., Roi, B. Le, Kamm, R. D. & Maoz, B. M. Biology and Models of the Blood-Brain barrier. *Annu Rev Biomed Eng* (2021).
129. Tan, H. Y. *et al.* A multi-chamber microfluidic intestinal barrier model using Caco-2 cells for drug transport studies. *PLoS One* **13**, (2018).

130. Yang, X., Pabon, L. & Murry, C. E. Engineering adolescence: Maturation of human pluripotent stem cell-derived cardiomyocytes. *Circ. Res.* **114**, 511–523 (2014).
131. Zwi, L. *et al.* Cardiomyocyte differentiation of human induced pluripotent stem cells. *Circulation* **120**, 1513–1523 (2009).
132. van Meer, B. J., Tertoolen, L. G. J. & Mummery, C. L. Measuring Physiological Responses of Human Pluripotent Stem Cell Derived Cardiomyocytes to Drugs and Disease. *Stem Cells* **34**, 2008–2015 (2016).
133. Brandao, K. O., Tabel, V. A., Atsma, D. E., Mummery, C. L. & Davis, R. P. Human pluripotent stem cell models of cardiac disease: From mechanisms to therapies. *Dis. Model. Mech.* **10**, 1039–1059 (2017).
134. Gaio, N. *et al.* Cytostretch, an Organ-on-Chip platform. *Micromachines* **7**, (2016).
135. Shin, H. *et al.* 3D high-density microelectrode array with optical stimulation and drug delivery for investigating neural circuit dynamics. *Nat. Commun.* **12**, (2021).
136. Blau, A. *et al.* Flexible, all-polymer microelectrode arrays for the capture of cardiac and neuronal signals. *Biomaterials* **32**, 1778–1786 (2011).
137. Soscia, D. A. *et al.* A flexible 3-dimensional microelectrode array for in vitro brain models. *Lab Chip* **20**, 901–911 (2020).
138. van Meer, B. J., Tertoolen, L. G. J. & Mummery, C. L. Measuring physiological responses of human pluripotent stem cell derived cardiomyocytes to drugs and disease. *Stem Cells* **34**, 2008–2015 (2016).
139. Sender, R. & Milo, R. The distribution of cellular turnover in the human body. *Nat. Med.* **27**, 45–48 (2021).
140. Tatsuya Osaki, Serrano, J. C. & Kamm, R. D. Cooperative Effects of Vascular Angiogenesis and Lymphangiogenesis. *Regen Eng Transl Med* **4**, 120–132 (2018).
141. Eddington, D. T., Puccinelli, J. P. & Beebe, D. J. Thermal aging and reduced hydrophobic recovery of polydimethylsiloxane. *Sensors Actuators, B Chem.* **114**, 170–172 (2006).
142. van Meer, B. J. *et al.* Small molecule absorption by PDMS in the context of drug response bioassays. *Biochem. Biophys. Res. Commun.* **482**, 323–328 (2017).
143. Lamberti, A., Marasso, S. L. & Cocuzza, M. PDMS membranes with tunable gas permeability for microfluidic applications. *RSC Adv.* **4**, 61415–61419 (2014).
144. Firpo, G., Angeli, E., Repetto, L. & Valbusa, U. Permeability thickness dependence of polydimethylsiloxane (PDMS) membranes. *J. Memb. Sci.* **481**, 1–8 (2015).
145. O'Brien, D. J. *et al.* Systematic Characterization of Hydrophilized Polydimethylsiloxane. *J. Microelectromechanical Syst.* **29**, 1216–1224 (2020).
146. Nakano, H., Kakinoki, S. & Iwasaki, Y. Long-lasting hydrophilic surface generated on poly(dimethyl siloxane) with photoreactive zwitterionic polymers. *Colloids Surfaces B Biointerfaces* **205**, (2021).
147. Holczer, E. & Fürjes, P. Effects of embedded surfactants on the surface properties of PDMS; applicability for autonomous microfluidic systems. *Microfluid. Nanofluidics* **21**, (2017).
148. McMillan, A. H. *et al.* Rapid fabrication of membrane-integrated thermoplastic elastomer microfluidic devices. *Micromachines* **11**, (2020).
149. Lachaux, J. *et al.* Thermoplastic elastomer with advanced hydrophilization and bonding performances for rapid (30 s) and easy molding of microfluidic devices. *Lab Chip* **17**, 2581–2594 (2017).
150. Busek, M. *et al.* Thermoplastic elastomer (TPE)–poly(methyl methacrylate) (PMMA) hybrid devices for active pumping PDMS-free organ-on-a-chip systems. *Biosensors* **11**, (2021).
151. Kim, D. S., Jeong, Y. J., Lee, B. K., Shanmugasundaram, A. & Lee, D. W. Piezoresistive sensor-integrated PDMS cantilever: A new class of device for measuring the drug-induced changes in the mechanical activity of cardiomyocytes. *Sensors Actuators, B Chem.* **240**, 566–572 (2017).
152. Lind, J. U. *et al.* Instrumented cardiac microphysiological devices via multimaterial three-dimensional printing. *Nat. Mater.* **16**, 303–308 (2017).
153. Coln, E. A. *et al.* Piezoelectric bioMEMS cantilever for measurement of muscle contraction and for actuation of mechanosensitive cells. *MRS Commun.* **9**, 1186–1192 (2019).
154. Wang, Y. & Sugino, T. *Ionic Polymer Actuators: Principle, Fabrication and Applications*. *Actuators* (2018). doi:10.5772/intechopen.75085.
155. Mastrangeli, M. *et al.* Microelectromechanical Organs-on-Chip. *21st Int. Conf. Solid-State Sensors, Actuators Microsystems, TRANSDUCERS 2021* 102–107 (2021) doi:10.1109/Transducers50396.2021.9495646.
156. Mirfakhrai, T., Madden, J. D. W. & Baughman, R. H. Polymer artificial muscles. *Mater. Today* **10**, 30–38 (2007).

157. Annabestani, M. & Fardmanesh, M. Ionic Electro active Polymer-Based Soft Actuators and Their Applications in Microfluidic Micropumps, Microvalves, and Micromixers: A Review. in *arXiv* (2019).
158. Osaki, T., Uzel, S. G. M. & Kamm, R. D. Microphysiological 3D model of amyotrophic lateral sclerosis (ALS) from human iPS-derived muscle cells and optogenetic motor neurons. *Sci. Adv.* **4**, (2018).
159. Gerasimenko, T. *et al.* Impedance Spectroscopy as a Tool for Monitoring Performance in 3D Models of Epithelial Tissues. *Front. Bioeng. Biotechnol.* **7**, (2020).
160. van der Helm, M. W. *et al.* Non-invasive sensing of transepithelial barrier function and tissue differentiation in organs-on-chips using impedance spectroscopy. *Lab Chip* **19**, 452–463 (2019).
161. Groeber, F. *et al.* Impedance Spectroscopy for the Non-Destructive Evaluation of in Vitro Epidermal Models. *Pharm. Res.* **32**, 1845–1854 (2015).
162. Yeste, J. *et al.* Geometric correction factor for transepithelial electrical resistance measurements in transwell and microfluidic cell cultures. *J. Phys. D. Appl. Phys.* **49**, (2016).
163. Blume, L. F., Denker, M., Gieseler, F. & Kunze, T. Temperature corrected transepithelial electrical resistance (TEER) measurement to quantify rapid changes in paracellular permeability. *Pharmazie* **65**, 19–24 (2010).
164. Grimnes, S. & Martinsen, Ø. G. Sources of error in tetrapolar impedance measurements on biomaterials and other ionic conductors. *J. Phys. D. Appl. Phys.* **40**, (2007).
165. Bossink, E. G. B. M., Zakharova, M., De Bruijn, D. S., Odijk, M. & Segerink, L. I. Measuring barrier function in organ-on-chips with cleanroom-free integration of multiplexable electrodes. *Lab Chip* **21**, 2040–2049 (2021).
166. Matthiesen, I., Voulgaris, D., Nikolakopoulou, P., Winkler, T. E. & Herland, A. Continuous Monitoring Reveals Protective Effects of N-Acetylcysteine Amide on an Isogenic Microphysiological Model of the Neurovascular Unit. *Small* **17**, (2021).
167. Maoz, B. M. *et al.* Organs-on-Chips with combined multi-electrode array and transepithelial electrical resistance measurement capabilities. *Lab Chip* **17**, 2294–2302 (2017).
168. Liu, F., Ni, L. & Zhe, J. Lab-on-a-chip electrical multiplexing techniques for cellular and molecular biomarker detection. *Biomicrofluidics* **12**, (2018).
169. Curto, V. F., Ferro, M. P., Mariani, F., Scavetta, E. & Owens, R. M. A planar impedance sensor for 3D spheroids. *Lab Chip* **18**, 933–943 (2018).
170. Schmid, Y. R. F., Bürgel, S. C., Misun, P. M., Hierlemann, A. & Frey, O. Electrical Impedance Spectroscopy for Microtissue Spheroid Analysis in Hanging-Drop Networks. *ACS Sensors* **1**, 1028–1035 (2016).
171. Alexander, F., Eggert, S. & Price, D. Label-Free Monitoring of 3D Tissue Models via Electrical Impedance Spectroscopy. *Bioanal. Rev.* **2**, 111–134 (2019).
172. Moysidou, C. M. *et al.* 3D Bioelectronic Model of the Human Intestine. *Adv. Biol.* **5**, (2021).
173. Zhu, Y. *et al.* State of the art in integrated biosensors for organ-on-a-chip applications. *Curr. Opin. Biomed. Eng.* **19**, (2021).
174. Kieninger, J., Weltin, A., Flamm, H. & Urban, G. A. Microsensor systems for cell metabolism-from 2D culture to organ-on-chip. *Lab Chip* **18**, 1274–1291 (2018).
175. Oliveira, M., Conceição, P., Kant, K., Ainla, A. & Diéguez, L. Electrochemical sensing in 3d cell culture models: New tools for developing better cancer diagnostics and treatments. *Cancers (Basel).* **13**, (2021).
176. Aleman, J., Kilic, T., Mille, L. S., Shin, S. R. & Zhang, Y. S. Microfluidic integration of regeneratable electrochemical affinity-based biosensors for continual monitoring of organ-on-a-chip devices. *Nat. Protoc.* **16**, 2564–2593 (2021).
177. Zhang, Y. S. *et al.* Multisensor-integrated organs-on-chips platform for automated and continual in situ monitoring of organoid behaviors. *Proc. Natl. Acad. Sci. U. S. A.* **114**, (2017).
178. Kaisti, M. Detection principles of biological and chemical FET sensors. *Biosens. Bioelectron.* **98**, 437–448 (2017).
179. Usuba, R. *et al.* Photonic Lab-on-a-Chip for Rapid Cytokine Detection. *ACS Sensors* **1**, 979–986 (2016).
180. Narang, R. *et al.* Sensitive, Real-time and Non-Intrusive Detection of Concentration and Growth of Pathogenic Bacteria using Microfluidic-Microwave Ring Resonator Biosensor. *Sci. Rep.* **8**, (2018).
181. Shaegh, S. A. M. *et al.* A microfluidic optical platform for real-time monitoring of pH and oxygen in microfluidic bioreactors and organ-on-chip devices. *Biomicrofluidics* **10**, (2016).
182. Luchansky, M. S. & Bailey, R. C. Rapid, multiparameter profiling of cellular secretion using silicon photonic microring resonator arrays. *J. Am. Chem. Soc.* **133**, 20500–20506 (2011).
183. Podoleanu, A. G. Optical coherence tomography. *J. Microsc.* **247**, 209–219 (2012).

184. Braaf, B. *et al. OCT-Based Velocimetry for Blood Flow Quantification*. *High Resolution Imaging in Microscopy and Ophthalmology* (2019). doi:10.1007/978-3-030-16638-0_7.
185. Arik, Y. B. *et al.* Microfluidic organ-on-a-chip model of the outer blood-retinal barrier with clinically relevant read-outs for tissue permeability and vascular structure. *Lab Chip* **21**, 272–283 (2021).
186. Pauty, J. *et al.* A Vascular Endothelial Growth Factor-Dependent Sprouting Angiogenesis Assay Based on an In Vitro Human Blood Vessel Model for the Study of Anti-Angiogenic Drugs. *EBioMedicine* **27**, 225–236 (2018).
187. Dalmay, C. *et al.* Ultra sensitive biosensor based on impedance spectroscopy at microwave frequencies for cell scale analysis. *Sensors Actuators, A Phys.* **162**, 189–197 (2010).
188. Artis, F. *et al.* Microwaving biological cells: Intracellular analysis with microwave dielectric spectroscopy. *IEEE Microw. Mag.* **16**, 87–96 (2015).
189. Grenier, K. *et al.* Recent advances in microwave-based dielectric spectroscopy at the cellular level for cancer investigations. *IEEE Trans. Microw. Theory Tech.* **61**, 2023–2030 (2013).
190. Kelleci, M., Aydogmus, H., Aslanbas, L., Erbil, S. O. & Selim Hanay, M. Towards microwave imaging of cells. *Lab Chip* **18**, 463–472 (2018).
191. Jang, C., Park, J.-K., Lee, H.-J., Yun, G.-H. & Yook, J.-G. Sensitivity-Enhanced Fluidic Glucose Sensor Based on a Microwave Resonator Coupled With an Interferometric System for Noninvasive and Continuous Detection. *IEEE Trans Biomed Circuits Syst* **15**, 1017–1026 (2021).
192. Zarifi, M. H., Sadabadi, H., Hejazi, S. H., Daneshmand, M. & Sanati-Nezhad, A. Noncontact and Nonintrusive Microwave-Microfluidic Flow Sensor for Energy and Biomedical Engineering. *Sci. Rep.* **8**, (2018).
193. Wikswo, J. P. *et al.* Scaling and systems biology for integrating multiple organs-on-a-chip. *Lab Chip* **13**, 3496–3511 (2013).
194. Herland, A. *et al.* Quantitative prediction of human pharmacokinetic responses to drugs via fluidically coupled vascularized organ chips. *Nat. Biomed. Eng.* **4**, 421–436 (2020).

Supplementary information

Contents

1 Methodology

The current review is the outcome of the Netherlands Organ-on-Chip Initiative, a program with specific interest in developing advanced OoC systems for the vasculature, intestine, heart and brain. The decision to focus on the vasculature, intestine, heart and brain was developmentally driven: including derivatives of all three germlayers, an endodermal (intestine), ectodermal (brain) and mesodermal (heart) organ, with the vasculature as a link to all.

The review was based on the following stepwise approach:

1. Determine the specific physiological features of each organ of interest. Of note: for each selected organ, we discuss an extensive but not exhaustive list of physiological features that have been quantitatively modelled in MPS. In addition, for some features, the implications for a specific MPS can be extrapolated to other organs.

2. Identify literature describing MPS of each selected organ that meets the following criteria;
   - The model system falls within our MPS definition. A broad and inclusive definition of MPS was adopted, to capture all of those relevant for the four organs selected. Microdevices containing cells in 2D or 3D cultures that either replicate the mechanical microenvironment by integrating fluid flow or mechanical actuation, or that integrate sensing modalities. We included systems that employ direct cell culture inside microfluidic or actuating systems, as well as those that integrate pre-engineered 3D tissues in these systems. The majority of discussed systems are microfluidic systems, which we refer to as Organ-on-Chip (OoC). Exceptions to this definition are clearly indicated in the text with the reason of inclusion. We excluded organoid cultures, since their stochastic, self-organizing nature generally precludes controlled confinement, and systems that model organ-organ connections in light of our focus on organ-specific features.
   - Reports accurate quantification of one of the defined physiological features of an organ or tissue in a healthy state. We focused on quantification of a healthy organ or tissue as this provides a baseline for comparing aberrant organ functions in disease.
   - Human cells were used in the system (primary, immortalized or iPSC-derived). Exceptions in which uses animal cells in a MPS are clearly indicated in the text.

3. Extract quantitative MPS values from the papers

4. Determine the best example to highlight. Selection was based on the most accurate quantification method, comparability with *in vivo* observations, the most suitable MPS type or an example which highlights an important consideration regarding quantification of that specific physiological feature.

5. Search for and extract, whenever possible, *in vivo* quantification of the specific physiological feature in human tissue. If human observations *in vivo* were not available, we sometimes included animal data. The result of these steps can be seen in *Table 1* and Supplemental table 1.

6. Identify technical advances which could overcome limitations in the current quantification methods of each physiological feature. Applicable technologies for MPS were considered which could improve quantification by either increasing the accuracy of measurement or improving the *in vivo* comparability. The proposed advances were grouped into several overarching technological areas to enable a more general overview on MPS technology and its areas of potential improvement.

2 Organ physiology and biological features of the human vasculature, intestine, heart and brain

Physiological features can be divided into 'designed' (blue) and 'emergent' (red) (*Supplemental figure 1*). Features may belong to either or both groups depending on the specific model and functional read-out required. In this review, they are divided for simplicity into one of the categories depending on the context discussed in this review. Microphysiological systems (MPS) can quantitatively control and monitor physiological features. Accurate quantification of these features is essential for system-to-system comparisons and understanding *in vivo* relevance which will facilitate development of measurable standards to designate a system as 'fit for purpose'. Here, we describe the basic organ physiology and biological features for the human vasculature, intestine, heart and brain (*Supplemental figure 1*).

Vasculature. Blood vessels are cylindrical tubes with diverging diameters which transport oxygen and nutrients through the body and remove waste products. The vessel wall consists of a single layer of endothelial cells surrounded by either smooth muscle cells or pericytes, depending on tissue location. There is also broad molecular heterogeneity within the vascular bed depending on the position in the vascular tree and the microenvironment of the surrounding tissue. Vascular cells sense and respond to many biomechanical and biochemical cues. Hemodynamic forces such as wall shear stress and circumferential strain or exerted by interstitial flow, tissue elasticity and the local oxygen concentration are examples of such cues. Blood vessels can actively respond to these signals by contracting or dilating (vascular reactivity), forming new blood vessels from those pre-existing (angiogenesis), or adjusting barrier integrity between the blood and the surrounding tissue to transport cytokines, hormones and other plasma constituents. Among the most important functions of blood vessels is responding to inflammatory stimuli by secreting cytokines and enabling immune cell transmigration.

Intestine. The intestine digests and selectively transports nutrients from its lumen to the bloodstream (small intestine) and absorbs remaining water and salts (large intestine). The enormous absorption capacity is related to the specific organization of the epithelial lining into finger-like structures (villi) and crypts, which increase the effective surface area. Epithelial cells start as stem cells in the crypts, migrate along the villus while maturing into functional cells and reach the tip of the villus after 3-4 days, which marks the end of their life cycle. They are organized along the villi according to their function (e.g. production of digestive enzymes, hormones and mucus along the villus length; epithelial regeneration and production of anti-microbial peptides in the crypt). The uptake of nutrients and transport of waste is facilitated by the mechanical microenvironment: peristaltic motion caused by a layer of longitudinal and circular (smooth) muscle cells resulting in continuous flow of luminal content. The intestine is also an important barrier that actively controls the transport of luminal content to the circulatory system. The mucus layer forms the first mechanical barrier, followed by the tight epithelial layer that maintains barrier integrity

and intestinal homeostasis. Immune cell surveillance of the epithelial barrier determines whether tolerance is maintained or inflammation elicited in response to digested and transported macromolecules. Oxygen gradients from the small- to the large intestine and from the lumen to the *lamina propria* allows survival of specific commensal microorganisms in each region without compromising the survival of adjacent intestinal epithelial cells. The commensal microorganisms that thrive in the anaerobic environment of the intestine are essential for both digestion and regulation of the intestinal immune response.

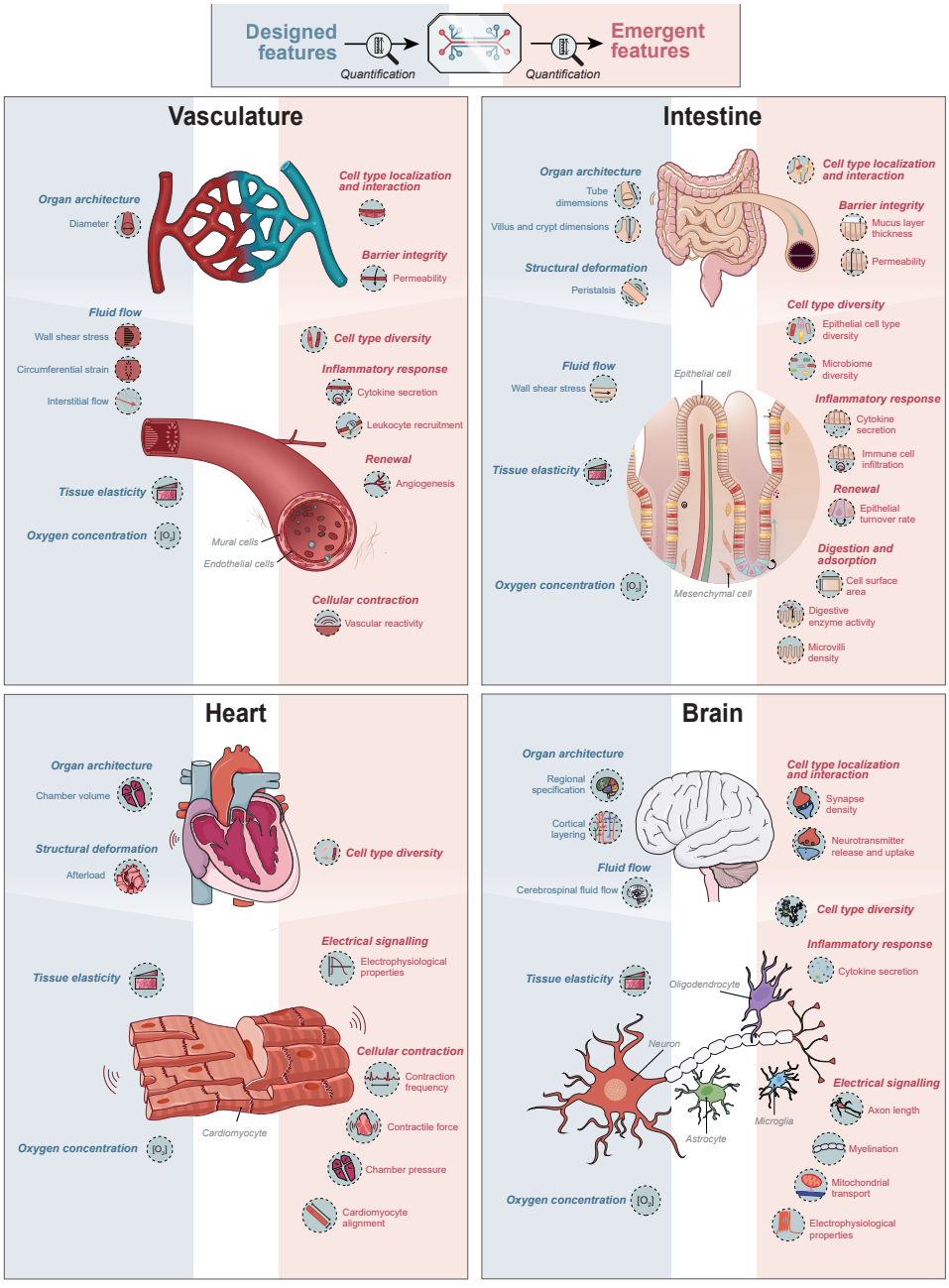

Supplemental figure 1: Schematic overview of physiological features of four selected organs: human vasculature, intestine, heart and brain. *Features may belong to either or both groups depending on the specific model and functional read-out required.*

Heart. The heart pumps blood through the vasculature to distribute oxygen and nutrients and remove carbon dioxide and metabolic waste. It consists of four chambers (two upper atrial chambers and two lower ventricular chambers), which synchronously pump blood to either the lungs or rest of the body using valves to prevent blood backflow. It is made up of the contractile cardiomyocytes and multiple non-cardiomyocyte cell types such as fibroblasts, endothelial-, endocardial-, epicardial-, neuronal and immune cells. The sinoatrial node, which acts as the pacemaker, works in combination with the atrioventricular node and the Purkinje fibers to propagate electrical signals throughout the myocardial wall regulating cardiomyocyte contraction. The resulting contractile frequency and force are highly dependent on the cellular organization (e.g. coupling, alignment) of the cardiomyocytes and other cell types. Resident fibroblasts ensure the extracellular matrix (ECM) is well-maintained via protein turnover, thus controlling heart tissue elasticity. In the heart, varying (or reduced) oxygen concentrations are key in the onset or development of cardiac disease, as in myocardial infarction.

Brain. The human brain is organized in distinct functional and structural domains: the cerebrum, cerebellum and brainstem. Different brain regions, such as the hippocampus, cerebellum and the prefrontal cortex, have distinct topographical structures. Higher cognitive functioning is thought to arise from the prefrontal cortex, a layered sheet of neural tissue with topographic separation into functional domains. Each brain region and neural cell type are distinct in their function and interaction, ensuring proper brain function. Besides blood flow, the brain is perfused by cerebrospinal fluid. This fluid is continuously produced by the choroid plexus and is involved in the distribution of nutrients and clearance of waste products. The brain is a highly active organ, so adequate oxygen levels are essential for maintaining proper brain function. At a cellular level, diverse neuronal subtypes and glial cells, such as astrocytes, microglia and oligodendrocytes, form neural networks that produce the brain output. Neurons communicate via these neural networks between- and within brain regions by propagating electrical signals (action potentials) along their axons, ultimately transmitting these through synapses using various neurotransmitters. This energy-consuming process requires mitochondrial anterograde transport along the axons for molecules and ions to reach the axon terminal, whereas retrograde transport is important for removing damaged organelles and debris. Astrocytes promote neuronal maturation and synapse development, maintain the blood-brain-barrier, provide neurons with metabolites and govern network activity. Oligodendrocytes produce an insulating layer, myelin, around the axons of neurons, ensuring efficient propagation of action potentials. The brain is a soft organ, more than 20% of this organ is made up of ECM, providing a scaffold for neural cells to migrate and make connections to other brain regions. Upon injury, microglia and astrocytes release and respond to inflammatory cytokines, creating scar tissue and removing debris from the extracellular space.

3 General designed features: Cell source and media

Two designed features relevant for any *in vitro* model are the cell source and cell culture medium used. These features largely influence the emergent features.

Cell source

The most commonly used cell sources are primary human cells (either commercially available or patient-derived) or immortal(ized) or cancer cell lines since they are generally easy-to-use. All three are inexpensive and can show features of their tissue or organ source[1]. More recently, advances in stem cell biology enabled increasing application of either adult human stem cells (most easily derived from endodermal organs) or human induced pluripotent stem cells (hiPSCs) which are derived by reprogramming somatic cells to a state from which they can form derivatives of all organs[2]. hiPSC lines can be generated from healthy individuals or patients with genetic disorders and can be genetically engineered to introduce- or remove disease-specific mutations or variants for disease modelling[1]. They can also be geneticlally modified to incorporate cell type-specific (fluorescent) reporter constructs or phenotypic sensors. Drawbacks include cost, operator skill and an often immature phenotype although the latter can for some cells be obviated by inclusion in the MPS.

Media composition

MPS provide complex culture systems often with the inclusion of multiple tissue cell types from any of the sources above. Maintaining tissue-specific cell types requires the correct combination of nutrients, metabolites and growth factors. Blood vessels would normally be exposed to blood; cells in organs are generally either exposed to interstitial fluid or components of blood that have passed through the blood vessel wall. However, most current MPS have limited compatibility with physiological perfusates, such as whole blood, and there is to date no universal medium that can serve as a 'blood mimetic'[3]. Current MPS usually address this by either mixing media with different compositions that support the individual cell types in the system and examining the outcome empirically, or by compartmentalizing the device to 'feed' different cell types independently.

4. Supplemental Table 1|Quantification of designed and emergent physiological features in microphysiological systems and human in vivo

Category	Organ	Feature	MPS		In vivo (human)	Ref MPS	Ref In Vivo
			Method	Quantification	Quantification		
Fluid flow	Vessel	Interstitial flow	Pressure pump	1.3 µm/s	0.1-2 µm/s (rabbit)	4	5
Cell type diversity	Intestine	Microbiome – bacterial diversity	CFU count; 16S rRNA sequencing	118-135 OTUs (primary cells, Ileum) and 200 OTUs (Caco-2)	280 OTUs	6	7
Inflammatory response	Vessel	Patrolling monocyte speed	Real-time fluorescent imaging	3-12 µm/min	9-36 µm/min (mouse)	8	9
	Intestine	Immune cell infiltration	IF	22-25 CD103+ cells /µm^2 in epithelial layer upon LPS stimulation	≤ 25 IELs / 100 epithelial cells (Duodenum, healthy)	10	11
Barrier integrity	Intestine	Mucus layer thickness	Dark field microscopy and beads	Outer layer: 370 µm, inner layer: 200 µm	SI: 50-450 µm; LI: outer layer 300-700 µm, inner layer 100-400 µm	12	13
Electrical signaling	Brain	Axon length	Compartmentalized system	9 - 12 cm	> 1 meter	14	15
		Myelin thickness	Electron microscopy on compartmentalized system	Average G-ratio of 0.57 ± 0.16	G-ratio of 0.68-0.8	16	17
		Myelin length	IF and artificial 'axons'	10 - 120 µm	18.28-57.36 µm (mouse)	18	19
		Axonal transport speed of mitochondria	Directed axonal growth in compartmentalized system	0.6 µm/s	0.22 µm/s (mouse)	20	21

4. Supplemental Table 1|continued

Category	Organ	Feature	MPS		In vivo (human)	Ref MPS	Ref In Vivo
			Method	Quantification	Quantification		
Cellular contraction	Heart	Contraction frequency	Video tracking	55-80 BPM	~64 BPM	22	23
			Video tracking	43-57 BPM		24	
			Pillar tracking	32 BPM		25	
		Contractile force	Pillar tracking	6.2 ± 0.8 mN/mm^2	44 mN/mm^2	26	27
			Pillar tracking	~12.5 µN		28	
			Pillar tracking	~3 mN/mm^2		29	
		Force Frequency Relationship	Video tracking	Positive	Positive	28	30
		Cardiomyocyte Alignment	Optical imaging	88-96/12.5-13.5 µm (Aspect ratio: 7.6±0.4:1)	141/19 µm (aspect ratio: 7.4:1)	26	31
		Systolic ventricular pressure	Intraventricular pressure sensor	50 µmHg	120 mmHg	32	33

4. Supplemental Table 1|continued

Category	Organ	Feature	MPS		In vivo (human)	Ref MPS	Ref In Vivo
			Method	Quantification	Quantification		
Digestion and absorption	Intestine	Cell surface area	Imaging and computational 3D reconstructions	Enlargement factor (apical cell surface compared to monolayer): 1.7-fold (excluding microvilli)	Enlargement factor villi: 4.5-8.6 (SI). Enlargement factor microvilli: 9.2-15.7 (SI), 6.4-6.7 (LI)	34	35, 36
		Microvilli density	SEM and ImageJ	7/μm^2	Jejunum: 114/μm^2 (Villus crest), 22/μm^2 (Intervillus space), 15/μm2 (Crypt)	37	38
		Glucose uptake rate	Quantification of glucose in medium	~280 mmol L^{-1} h^{-1}, ~0.3 nmol $cell^{-1}$ h^{-1}	Vmax= 83/25 mmol/h/15-cm segment and Km= 154/50 mmol/L (Jejunum/Ileum)	34	39
		Digestive enzyme activity	Aminopeptidase activity assay, A4N	9, 12 fmol/min/cell (flow, flow and strain)	NA	40	
				0.92 fmol/min/cell		41	
			Sucrase-isomaltase activity assay (30 mM sucrose to glucose)	15-40 U/g protein	Vmax=83/36 mmol/h/15-cm segment and Km=142/74 mmol/L (Jejunum/Ileum)	42	39
		Drug metabolizing enzyme activity	LC-MS of metabolized drug in outflow (testosterone to 6β-OH-T)	0.056 nmol/min/mg protein	0.36-2.46 nmol/min/mg protein (Jejunum)	37	43

Data was included based on the criteria as stated in Supplement Methodology 1.2. Abbreviations: MPS=microphysiological system, NA=not available, SI=small intestine, LI=large intestine, IEL=intraepithelial lymphocyte, CFU=colony-forming unit, OTU=operational taxonomic unit, LC-MS=liquid chromatography-mass spectrometry, IF=immunofluorescence, LPS=lipopolysaccharide, 6β-OH-T=6β-hydroxytestosterone, m=meter, BPM=beats per minute, N=Newton, h=hour, min=minute, s=second, ref=reference.

5 Supplemental discussion designed feature

Fluid flow – interstitial flow

Interstitial flow describes the movement of fluid through the ECM and its resident cells and is the type of flow present in almost all tissues and organs. The forces exerted on cells by interstitial flow are more challenging to measure or calculate *in vivo* and *in vitro* and are therefore expressed as fluid flow speed. In the vasculature, interstitial flow has been described in great detail and it has been associated with vasculogenesis, lymphogenesis and lymphatic drainage of blood plasma which has leaked from the micro-vasculature. A similar process takes place in the brain, where cerebral spinal fluid (CSF), produced by cells of the choroid plexus, flows via the four ventricles of the brain to subarachnoid spaces, clearing waste products, distributing trophic factors and maintaining brain pH balance in the process[44]. OoCs have been able to model interstitial flow using 3D hydrogel compartments with known biophysical parameters suitable for convection of fluid at controllable velocities. In one technologically-advanced approach, a hydrogel containing a self-assembled vascular network was pressurized using a pump to apply constant interstitial flow[4]. Both computational simulation of flow velocities and verification using fluorescence recovery after photobleaching (FRAP) showed that interstitial flow was in the physiological range (*SI Table 1*). Interestingly, the device design also allowed direct sampling of the interstitial fluid enabling investigation of therapeutic molecule distribution. This type of system is suitable for use on tissues embedded in a hydrogel; however, it cannot be applied to free floating tissues in culture. This is exemplified by a BoC system which uses rat cortical neurospheroids to study the effect of flow on waste clearance and neuronal maturation. Here, an osmotic micropump was used to apply a constant flow of 0.15 µl/min over spheroids trapped in concave microwells at the bottom of the microfluidic channel[45]. Improved neuronal differentiation and synapse formation was observed within the neurospheroid, suggesting that a rudimentary model of CSF flow can already benefit neuronal maturation. As described, there are multiple technological solutions to create intersitial flow. Important for correct quantitative implementation of these forces is the correct verification within the system. Multiple methods can be used to do so, including computational simulation and FRAP as previously discussed for VoCs[4].

6 Supplemental discussion designed feature

Cell type diversity – microorganisms

Non-human cells, such as commensal microorganisms in the intestine, can be quantified using another type of analysis: 16S rRNA sequencing. This technique was used to quantify microbiome diversity in a GoC system[6] (SI *Table 1*). The healthy human microbiome is composed of ~200 species[46]. Modeling the microbiome *in vitro* thus requires a complex environment that supports many different species, with different needs in terms of oxygen concentration, nutrition and space. A GoC system containing over 200 unique operational taxonomic units (OTUs) from healthy human stool specimens was reportedly sustained for at least five days, comparing favorably with 280 OTUs in human intestinal aspirates[6]. Sequencing 16S rRNA is suitable to quantify microbial diversity in *in vitro* models, since the same methods can be used to characterize microbial diversity in intestinal brush border or stool samples. Alternatively, metagenomic sequencing provides insight in active microbial metabolic pathways and is applied to different areas of the human intestine to get insight into the contribution of location-specific microbiome niches.

Immune cell migration speed

Quantification of the number of transmigrated or infiltrated immune cells are clinically relevant proxies for the inflammatory and disease state[47]. The quantification of transmigrated or infiltrated immune cells requires normalization to the total tissue area analyzed[48,49]. This principle has been applied in both VoC and GoC systems. One VoC model quantified transmigration of neutrophils on a template-based vessel containing several cylindrical ECM-filled stacks with known volume[50]. Accordingly, the number of transmigrated neutrophils per tissue volume could be derived in a similar way as in mice. Also self-assembled 3D vascular networks have proven useful for investigating the dynamics of monocyte transmigration in real-time[51]. However, both models lack continuous perfusion and cannot be used to quantify flow-related parameters such as monocyte patrolling speed. This still requires more classical *in vitro* approaches; for example an endothelial cell monolayer under physiologically-relevant shear flow was used to quantify monocyte migration speed (3-12 μm/min); this was shown to be close to that in mice (*SI Table 1*)[8,9]. To increase *in vivo* relevance further, future VoC models should include fluid flow and appropriate tissue elasticity. The importance of this was shown recently in work combining hydrostatic pressure driven flow over microfluidic channels in a collagen-based ECM[52]. The former VoC work can be extended by analysis of the migration of immune cells through an endothelial cell layer into a tissue, as was done in a GoC system. This multi-cell type systems contained a microchannel with an intestinal epithelial cell layer membrane-separated from a microchannel with an endothelial cell layer and monocyte-derived macrophages and dendritic cells. Using this system the number of dendritic cells invading the epithelial layer upon LPS stimulation was quantified to be ~22-25 $CD103^+$ cells/μm^2 of the epithelial layer[10]. Essentially the same method is used to

study chronic inflammatory diseases. For example, to diagnose celiac disease, the number of invading inflammatory immune cells is measured in human intestinal biopsies. Of note, the units slightly differ making direct comparison difficult: for GoCs the number of immune cells/μm^2 of epithelial cell layer was reported, whilst for intestinal biopsies they reported the number of intraepithelial lymphocytes per 100 epithelial cells which circumvents the need to determine surface area (*SI Table 1*). A similar unit can be used to express invading immune cells in GoCs. To date, the number of HoC models that incorporate components of the immune system are limited and robust quantifications on inflammatory response are lacking.

Barrier integrity – Mucus layer

Several GoC studies have quantified mucus production, either as dissociated mucin proteins in flow-through fluid[6,42] or as mucus layer thickness after fixation[34], which alters mucus layer structure. Dark-field microscopy is a non-invasive alternative allows study of the mucus layer in live cultures over time[12]. The outer and inner mucus layers can be distinguished based on pore size using fluorescently-labelled beads. Their thickness was estimated as 370 µm and 200 µm, respectively after 14 days in a GoC containing primary colon tissue. The chip design used required the removal of thin layers of PDMS parallel to the channels and subsequent analysis of the chips on a glass slide. Altering device design or advanced imaging methods might overcome this limitation (see 'Technical advances' for advanced imaging).

Electrical activity – brain

Neurons in the brain show great diversity in axon length, extending away from the cell body, to establish connectivity within the brain and relay signals to the remainder of the body using motor neurons[15]. Modelling the extension of these long axons has been done using a compartmentalized microfluidic devices[14]. In these BoC devices, hiPSC-derived motor neurons grew as bundles of axon up to 9-12 cm in length. Whilst remarkably long, the neurons were nevertheless approximately 100-fold shorter than *in vivo* equivalents. To relay signals throughout these elongated cells effectively, action potential conduction velocity needs to be ensured. For this, neurons require both myelination of their axons and active transport of mitochondria along these axons. Robust modelling and quantification of myelination and the build-up of small lipid-rich insulators, has only been described in a few MPS platforms. Among these is a nerve-on-chip device which described myelination of peripheral motor-neuron axons by Schwann cells, during guided outgrowth of axons from 3D spheroids[16]. Importantly, the model could be directly compared with *in vivo* measurements by using the same method and unit (*SI Table 1*). Electron microscopy was used to quantify the G-ratio i.e. the ratio between the inner and the outer diameter of the myelin sheath as a measure of myelin thickness. The BoC value was slightly lower than the G-ratio described for the human central nervous system (*SI Table 1*). This fits the notion that G-ratios in the peripheral

nervous system are generally lower; however, these values have not been quantified *in vivo* to our knowledge. Another MPS of the brain was used to quantify myelin length in rat oligodendrocytes using immunofluorescent microscopy (*SI Table 1*)[18]. Values were similar to the myelin length in mouse brain[19]. Active transport of mitochondria was measured in BoCs with microtunnel-separated culture compartments for the neuronal *soma* and thus forcing directed axonal outgrowth through the microtunnels and enabling live tracking of the mitochondria. This set-up allowed anterograde and retrograde transport of mitochondria to be distinguished with rates around 0.6 µm/s, the same order of magnitude as *in vivo*[20] (*SI Table 1*).

Cellular contraction

Contraction is the functional output of muscle tissues. The heart relies on the synchronized and timely contraction of muscle cells to pump blood through the body. Alignment of contractile myocytes is essential in efficient unidirectional muscle contraction, therefore, it also serves as one output of *in vitro* maturity and increased physiological mimicry.

Alignment of muscle cells can be quantified using their aspect (length to width) ratio in the direction of contraction[53]. Aspect ratios can increase in response to the cardiomyocyte environment and mechanical or chemical signals[54–56]. For instance, in EHTs made in an oval cell culture chamber with standing pillars, cardiomyocyte alignment is induced by the chamber shape and subsequently by unidirectional load from the pillars. Aspect ratios of 7.6 ± 0.4 have been reported in EHTs which resembles that of healthy human adult myocardium[26] (*SI Table 1*).

The overall output of the contraction of the cells can be described by its frequency, force and the force-frequency relationship (FFR). Cardiac muscle contraction frequency or rate is measured in beats per minute (BPM). This is easily quantified in MPS of the heart, for example by video tracking, but varies based on mechanical environment, cell-source and medium composition. Nevertheless, identifying factors affecting beat rate can provide insight into human physiology and facilitate drug discovery. For instance, beta-adrenergic signaling affects beating frequency[57]: in a cantilever-based cardiac model, seeded with hiPSC-derived cardiomyocytes in a constrained gel, baseline beat-rates were close to those in human heart and increased by ±60% upon beta-adrenergic stimulation (*SI Table 1*). Importantly, many cardiac diseases or drug side effects manifest as arrythmias which can be detected by irregular beating.

Quantification of force is in most MPS of the heart only possible indirectly, optical displacement of cells being taken as a measure of contraction[58]. Other studies optically track anchoring points with known stiffness to calculate the force of contraction needed for their displacement. Pillars, wires, force-transducers or 2D-tissue strips are all used[29,59,60]. Recently, MPS of the heart that simultaneously measure contractile force and extracellular field potential have been described. Cardiomyocytes were cultured on a flexible electronic

parylene-SR film with integrated gold-electrodes; contraction deflected the thin, flexible film and this generated compressive strain which was transmitted to allow direct, real-time monitoring of the excitation-contraction coupling[61]. The maximum force measured *in vivo* and *in vitro* depends on the tissue cross-section. Tissue force is thus best normalized to cross-sectional area, in principle enabling *in vitro* and *in vivo* comparisons. Nonetheless, measuring force as a function of the displacement of anchoring points as in EHTs is still prone to variability caused by differences in height of the tissue suspension points, insufficient information on the mechanical properties of anchoring points and differences in cross-sectional areas. Therefore, anchoring the tissue to a calibrated force-transducer still gives the best comparison with adult myocardium. The highest force values reported to date for MPS of the heart containing hiPSC-derived cardiomyocytes is 6.2 ± 0.8 mN/mm^2, achieved using standing pillars with serum-free medium[26]. This is similar to human infant myocardial force but still lower than adult heart *in vivo* (*SI Table 1*). In addition to the maximum contraction force, dynamics in the contraction transient (e.g. contraction time, relaxation time) provide insight into the drug mechanism of action and report expected effect *in vivo*. For example, the myosin activator omecamtiv mecarbil has been shown to increase both force of contraction and contraction time in hiPSC-derived cardiomyocyte EHTs[62], predicting the positive inotropic response in patients. A large study across multiple platforms showed that hiPSC-derived cardiomyocytes cultured in 2D and 3D are high predictive when based on output parameters such as time to peak, relaxation- and contraction time[57].

Adult human myocardial muscle strips show increased force at higher beating frequencies i.e. a positive FFR. This is not the case in mouse, failing or fetal hearts[30]. EHTs show positive FFR values after metabolic or electrical conditioning[26,28]. Relatively high baseline frequencies of spontaneously beating EHTs can mask the FFR. For this reason, ivabradine, a 'funny current' inhibitor, has been used to reduce the spontaneous beat-rate of EHTs to reveal a positive FFR, which could increase to about 200% of the baseline force. Ultimately, force is needed *in vivo* to generate enough pressure to circulate the blood through the body which is a highly relevant clinical read-out. Several different HoC systems have been designed to generate such pressure by engineering chambers and measured this pressure to assess the physiological relevance of their system. A HoC modelling ventricular chambers was used to perform pressure-volume loop measurements in a bioreactor and determined a maximum pressure of 50 µmHg[32], still far from the 120 mmHg *in vivo*[33]. While measuring output pressure is easier to compare with clinical values than force of contraction, the models require more complex engineering and typically higher cell numbers.

Digestion and absorption

The main function of the small intestine is to digest and absorb nutrients as source of energy for the body. The architecture of the epithelial barrier of the small intestine sustains this function through villi and microvilli, which greatly increase the surface area for nutrient

breakdown and absorption into the bloodstream. The enterocytes, which form the main cell type of the small intestinal epithelial barrier, produce digestive- and drug metabolizing enzymes to enhance the bioavailability of food and drugs after oral intake.

In GoC devices, the epithelial cells can self-organize into 3D villus-like folds when exposed to continuous flow in the top and bottom channel. Computational 3D surface reconstruction based on microscopic Z-stack images showed a 2-fold increase in epithelial surface area within two days of seeding Caco-2 cells in the upper microchannel of a GoC system[34]. Increasing the microchannel height above 150 µm might have allowed the villi to grow closer to the ~700 µm described for human intestine and achieve the same 4.5-8.6 surface area enlargement (*SI Table 1*). The surface area is further enlarged by the presence of microvilli on the surface of enterocytes, quantified to range from ~15/µm^2 in the crypts to ~200/µm^2 on the villus tips in human intestinal biopsies. Microvilli are often shown on enterocytes in GoCs but are rarely quantified. Exceptionally, one GoC study did quantify the microvilli density on the apical surface of primary duodenal tissue using electron microscopy and found upon dynamic force ~7 microvilli per µm^2 [37]. This finding underlines the importance of quantification to further improve GoC systems and increase their physiological relevance.

Nutrient absorption by intestinal epithelial cells can be relatively easily measured in GoC systems. A GoC investigated glucose uptake rates by the intestinal epithelial barrier by perfusing glucose-containing medium through the apical channel and glucose-free medium through the basal channel, then quantifying the glucose concentrations at the channel outlets and the total number of epithelial cells in the system[34] (*SI Table 1*). Multiple GoC studies have measured the activity of digestive enzymes such as sucrase-isomaltase[42] and aminopeptidase[40,41]. Both aminopeptidase studies confirmed increased enzyme activity upon fluid flow, however the kinetics are difficult to correlate with *in vivo* measurements of enzyme activity, as these mainly quantify substrates or metabolites in the systemic bloodstream after processing by multiple organs. In contrast, *in vitro* studies usually investigate the conversion rate of a substrate into a metabolite in a specific tissue or step of metabolism. The same issue arises when quantifying drug metabolizing enzyme activity. In very few cases, *in vivo* enzyme kinetics are described for a tissue specifically and can be compared directly to *in vitro* values. In a GoC system containing primary duodenal tissue for example, CYP3A4 enzymes transformed testosterone to 6β-hydroxytestosterone (6β-OH-T) with a metabolic rate of 0.056 nmol/min/mg protein which is lower than *in vivo* testosterone hydroxylation levels in human jejunum[37,43] (*SI Table 1*). In contrast, other GoC studies used non-physiological substrates that are metabolized to fluorescent derivatives, which are not comparable with *in vivo* measurements. This illustrates the need for sets of validated reference compounds, for which the effects in the human body are well described. More complex GoC systems, linked to other organs, and *in silico* modeling may address this in the future and eventually allow relevant quantification of a more complete digestion and drug metabolism process.

7 Standardization and open platforms

Accurate comparisons of different MPS have become increasingly challenging as MPS use has grown and customized MPS designs have emerged. To achieve system-to-system and lab-to-lab comparability, standardization is required at multiple levels. Among these, agreement on methods for quantification of designed and emergent features in MPS is crucial to develop measurable standards applicable to (customized or commercial) MPS designs and platforms. This includes standardization of sensitivity and accuracy of the methods, reporting of data, and the use of reference compounds or methods that have been well-established *in vivo*. Developing MPS that can achieve measurable standards might require additional consensus on the materials and cells used, interfacing with existing lab infrastructure and various MPS, and operating strategies[63]. One approach that facilitates standardization is using MPS platforms with standardized interface that can accommodate and interconnect different types of MPS[64]. MPS platforms could incorporate the multiplicity of existing MPS within the uniformity of a familiar and standardized interface. Commercial platforms already partly offer this type of standardization. Other initiatives, such as the Translational Organ-on-Chip Platform (TOP)[65] and the Moore4Medical's Smart Multi-Well Plate[66], implement standardized constraints for chip geometry and interfaces[67], and may provide more generally applicable open technology platforms in which new MPS designs can be implemented interchangeably in 'plug-and-play' formats. These open technology platforms will enable the modular integration of sensors or use of existing laboratory equipment to generate quantitative read-outs of emergent features in MPS without having to develop tailored solutions for individual MPS platforms. It has been argued that, by embedding a variety of MPS with a uniform and standardized interface, MPS platforms could contribute to establishing more reproducible and lab-independent MPS practice, amenable to wider adoption by end users and regulatory acceptance. To facilitate this, MPS developers should inform the design of their devices with the standards for geometry and interfaces adopted in the MPS platforms, in a process that gradually converges towards eliciting a set of shared templates for MPS design. In this way, these platforms will aid in standardizing the design and operation of MPS and pave the way to multi-organ systems.

Supplementary references

1. Van Den Berg, A., Mummery, C. L., Passier, R. & Van der Meer, A. D. Personalised organs-on-chips: functional testing for precision medicine. *Lab Chip* **19**, 198–205 (2019).
2. Sharma, A., Sances, S., Workman, M. J. & Svendsen, C. N. Multi-lineage Human iPSC-Derived Platforms for Disease Modeling and Drug Discovery. *Cell Stem Cell* **26**, 309–329 (2020).
3. Low, L. A., Mummery, C. L., Berridge, B. R., Austin, C. P. & Tagle, D. A. Organs-on-chips: into the next decade. *Nat. Rev. Drug Discov.* (2020) doi:10.1038/s41573-020-0079-3.
4. Offeddu, G. S. *et al.* Application of Transmural Flow Across In Vitro Microvasculature Enables Direct Sampling of Interstitial Therapeutic Molecule Distribution. *Microcirculation-on-Chip* **1902393**, (2019).
5. Swartz, M. A. & Fleury, M. E. Interstitial flow and its effects in soft tissues. *Annu. Rev. Biomed. Eng.* **9**, 229–256 (2007).
6. Jalili-firoozinezhad, S. *et al.* A complex human gut microbiome cultured in an anaerobic intestine-on-a-chip. *Nat. Biomed. Eng.* **3**, 520–531 (2019).
7. Villmones, H. C. *et al.* Species Level Description of the Human Ileal Bacterial Microbiota. *Sci. Rep.* **8**, (2018).
8. Collison, J. L., Carlin, L. M., Eichmann, M., Geissmann, F. & Peakman, M. Heterogeneity in the Locomotory Behavior of Human Monocyte Subsets over Human Vascular Endothelium In Vitro. *J. Immunol.* **195**, 1162–1170 (2015).
9. Buscher, K., Marcovecchio, P., Hedrick, C. C. & Ley, K. Patrolling Mechanics of Non-Classical Monocytes in Vascular Inflammation. *Front. Cardiovasc. Med.* **4**, (2017).
10. Maurer, M. *et al.* A three-dimensional immunocompetent intestine-on-chip model as in vitro platform for functional and microbial interaction studies. *Biomaterials* **220**, (2019).
11. Hayat, M., Cairns, A., Dixon, M. F. & O'Mahony, S. Quantitation of intraepithelial lymphocytes in human duodenum: what is normal? *J. Clin. Pathol.* **55**, 393–395 (2002).
12. Sontheimer-Phelps, A. *et al.* Human Colon-on-a-Chip Enables Continuous In Vitro Analysis of Colon Mucus Layer Accumulation and Physiology. *Cell Mol Gastroenterol Hepatol.* **9**, 507–526 (2020).
13. Dutton, J. S., Hinman, S. S., Kim, R., Wang, Y. & Allbritton, N. L. Primary Cell-Derived Intestinal Models: Recapitulating Physiology. *Trends Biotechnol.* **37**, 744–760 (2019).
14. Spijkers, X. M. *et al.* A directional 3D neurite outgrowth model for studying motor axon biology and disease. *Sci. Rep.* **11**, 2080 (2021).
15. Stifani, N. Motor neurons and the generation of spinal motor neuron diversity. *Front. Cell. Neurosci.* **8**, (2014).
16. Sharma, A. D. *et al.* Engineering a 3D functional human peripheral nerve in vitro using the Nerve-on-a-Chip platform. *Sci. Rep.* **9**, (2019).
17. Cercignani, M. *et al.* Characterizing axonal myelination within the healthy population: a tract-by-tract mapping of effects of age and gender on the fiber g-ratio. *Neurobiol. Aging* **49**, 109–118 (2017).
18. Espinosa-Hoyos, D. *et al.* Engineered 3D-printed artificial axons. *Sci. Rep.* **8**, (2018).
19. Tomassy, G. S. *et al.* Distinct Profiles of Myelin Distribution Along Single Axons of Pyramidal Neurons in the Neocortex. *Science (80-.).* **344**, 319–324 (2014).
20. Lu, X., Kim-Han, J. S., O'Malley, K. L. & Sakiyama-Elbert, S. E. A microdevice platform for visualizing mitochondrial transport in aligned dopaminergic axons. *J. Neurosci. Methods* **209**, 35–39 (2012).
21. Takihara, Y. *et al.* In vivo imaging of axonal transport of mitochondria in the diseased and aged mammalian CNS. *Proc. Natl. Acad. Sci. U. S. A.* **112**, 10515–10520 (2015).
22. Mathur, A. *et al.* Human iPSC-based cardiac microphysiological system for drug screening applications. *Sci. Rep.* **5**, 8883 (2015).
23. Drouin, E., Charpentier, F., Gauthier, C., Laurent, K. & Le Marec, H. Electrophysiologic characteristics of cells spanning the left ventricular wall of human heart: Evidence for presence of M cells. *J. Am. Coll. Cardiol.* **26**, 185–192 (1995).
24. Tulloch, N. L. *et al.* Growth of engineered human myocardium with mechanical loading and vascular coculture. *Circ. Res.* **109**, 47–59 (2011).
25. Mills, R. J. *et al.* Functional screening in human cardiac organoids reveals a metabolic mechanism for cardiomyocyte cell cycle arrest. *Proc. Natl. Acad. Sci.* **114**, E8372–E8381 (2017).
26. Tiburcy, M. *et al.* Defined engineered human myocardium with advanced maturation for applications in heart failure modeling and repair. *Circulation* **135**, 1832–1847 (2017).

27. Hasenfuss, G. *et al.* Energetics of isometric force development in control and volume-overload human myocardium. Comparison with animal species. *Circ. Res.* **68**, 836–846 (1991).
28. Zhao, Y. *et al.* Towards chamber specific heart-on-a-chip for drug testing applications. *Adv. Drug Deliv. Rev.* **165**–**166**, 60–76 (2020).
29. Ronaldson-Bouchard, K. *et al.* Advanced maturation of human cardiac tissue grown from pluripotent stem cells. *Nature* **556**, 239–243 (2018).
30. Wiegerinck, R. F. *et al.* Force frequency relationship of the human ventricle increases during early postnatal development. *Pediatr. Res.* **65**, 414–419 (2009).
31. Gerdes, A. M. *et al.* Structural remodeling of cardiac myocytes in patients with ischemic cardiomyopathy. *Circulation* **86**, 426–430 (1992).
32. MacQueen, L. A. *et al.* A tissue-engineered scale model of the heart ventricle. *Nat. Biomed. Eng.* **2**, 930–941 (2018).
33. Timmis, A. *et al.* European society of cardiology: Cardiovascular disease statistics 2019. *Eur. Heart J.* **41**, 12–85 (2020).
34. Kim, H. & Ingber, D. Gut-on-a-Chip microenvironment induces human intestinal cells to undergo villus differentiation. *Integr. Biol.* **5**, 1130–1140 (2013).
35. Helander, K. G., Åhren, C., Philipson, B. M., Samuelsson, B. M. & Ójerskog, B. Structure of mucosa in continent ileal reservoirs 15 to 19 years after construction. *Hum. Pathol.* **21**, 1235–1238 (1990).
36. Helander, H. F. & Fändriks, L. Surface area of the digestive tract-revisited. *Scand. J. Gastroenterol.* **49**, 681–689 (2014).
37. Kasendra, M. *et al.* Duodenum intestine-chip for preclinical drug assessment in a human relevant model. *Elife* **9**, (2020).
38. Brown, A. L. Microvilli of the human jejunal epithelial cell. *J Cell Biol.* **12**, 623–627 (1962).
39. Gray, G. M. & Ingelfinger, F. J. Intestinal absorption of sucrose in man: interrelation of hydrolysis and monosaccharide product absorption. *J. Clin. Invest.* **45**, 388–398 (1966).
40. Kim, H., Huh, D., Hamilton, G. & Ingber, D. Human gut-on-a-chip inhabited by microbial flora that experiences intestinal peristalsis-like motions and flow. *Lab Chip* **12**, 2165–2174 (2012).
41. Shim, K. Y. *et al.* Microfluidic gut-on-a-chip with three-dimensional villi structure. *Biomed. Microdevices* **19**, (2017).
42. Kasendra, M. *et al.* Development of a primary human Small Intestine-on-a-Chip using biopsy-derived organoids. *Sci. Rep.* **8**, (2018).
43. Obach, R. S., Zhang, Q. Y., Dunbar, D. & Kaminsky, L. S. Metabolic characterization of the major human small intestinal cytochrome P450S. *Drug Metab. Dispos.* **29**, 347–352 (2001).
44. Lun, M. P., Monuki, E. S. & Lehtinen, M. K. Development and functions of the choroid plexus-cerebrospinal fluid system. *Nat. Rev. Neurosci.* **16**, 445–457 (2015).
45. Park, J. *et al.* Three-dimensional brain-on-a-chip with an interstitial level of flow and its application as an in vitro model of Alzheimer's disease. *Lab Chip* **15**, 141–150 (2015).
46. Scepanovic, P. *et al.* A comprehensive assessment of demographic, environmental, and host genetic associations with gut microbiome diversity in healthy individuals. *Microbiome* **7**, 130 (2019).
47. Fajgenbaum, D. C. & June, C. H. Cytokine Storm. *N. Engl. J. Med.* **383**, 2255–2273 (2020).
48. Woodfin, A. *et al.* The junctional adhesion molecule JAM-C regulates polarized transendothelial migration of neutrophils in vivo. *Nat. Immunol.* **12**, 761–769 (2011).
49. Proebstl, D. *et al.* Pericytes support neutrophil subendothelial cell crawling and breaching of venular walls in vivo. *J. Exp. Med.* **209**, 1219–1234 (2012).
50. McMinn, P. H., Hind, L. E., Huttenlocher, A. & Beebe, D. J. Neutrophil trafficking on-a-chip: an in vitro, organotypic model for investigating neutrophil priming, extravasation, and migration with spatiotemporal control. *Lab Chip* **19**, 3697–3705 (2019).
51. Boussommier-Calleja, A. *et al.* The effects of monocytes on tumor cell extravasation in a 3D vascularized microfluidic model. *Biomaterials* **198**, 180–193 (2019).
52. Pérez-Rodríguez, S., Huang, S. A., Borau, C., García-Aznar, J. M. & Polacheck, W. J. Microfluidic model of monocyte extravasation reveals the role of hemodynamics and subendothelial matrix mechanics in regulating endothelial integrity. *Biomicrofluidics* **15**, (2021).
53. Bray, M. A., Sheehy, S. P. & Parker, K. K. Sarcomere alignment is regulated by myocyte shape. *Cell Motil. Cytoskeleton* **65**, 641–651 (2008).
54. Ribeiro, M. C. *et al.* Functional maturation of human pluripotent stem cell derived cardiomyocytes

invitro - Correlation between contraction force and electrophysiology. *Biomaterials* **51**, 138–150 (2015).
55. Ariyasinghe, N. R., Lyra-Leite, D. M. & McCain, M. L. Engineering cardiac microphysiological systems to model pathological extracellular matrix remodeling. *Am. J. Physiol. Circ. Physiol.* **315**, H771–H789 (2018).
56. Salick, M. R. *et al.* Micropattern width dependent sarcomere development in human ESC-derived cardiomyocytes. *Biomaterials* **35**, 4454–4464 (2014).
57. Saleem, U. *et al.* Blinded, Multicenter Evaluation of Drug-induced Changes in Contractility Using Human-induced Pluripotent Stem Cell-derived Cardiomyocytes. *Toxicol. Sci.* **176**, 103–123 (2020).
58. Marsano, A. *et al.* Beating heart on a chip: a novel microfluidic platform to generate functional 3D cardiac microtissues. *Lab Chip* **16**, 599–610 (2016).
59. Wijnker, P. J. M. *et al.* Comparison of the effects of a truncating and a missense MYBPC3 mutation on contractile parameters of engineered heart tissue. *J. Mol. Cell. Cardiol.* **97**, 82–92 (2016).
60. Grosberg, A., Alford, P. W., McCain, M. L. & Parker, K. K. Ensembles of engineered cardiac tissues for physiological and pharmacological study: Heart on a chip. *Lab Chip* **11**, 4165–4173 (2011).
61. Ohya, T. *et al.* Simultaneous measurement of contractile force and field potential of dynamically beating human iPS cell-derived cardiac cell sheet-tissue with flexible electronics. *Lab Chip* **21**, 3899–3909 (2021).
62. Saleem, U. *et al.* Force and Calcium Transients Analysis in Human Engineered Heart Tissues Reveals Positive Force-Frequency Relation at Physiological Frequency. *Stem Cell Reports* **14**, 312–324 (2020).
63. Piergiovanni, M., Leite, S. B., Corvi, R. & Whelan, M. Standardisation needs for organ on chip devices. *Lab Chip* **21**, 2857–2868 (2021).
64. Mastrangeli, M. *et al.* Building blocks for a European organ-on-chip roadmap. *ALTEX* **36**, 481–492 (2019).
65. Vollertsen, A. R. *et al.* Facilitating implementation of organs-on-chips by open platform technology. *Biomicrofluidics* **15**, (2021).
66. Mastrangeli, M. *et al.* Microelectromechanical Organs-on-Chip. *21st Int. Conf. Solid-State Sensors, Actuators Microsystems, TRANSDUCERS 2021* 102–107 (2021) doi:10.1109/Transducers50396.2021.9495646.
67. ISO 22916: 2022. Microfluidic devices — Interoperability requirements for dimensions, connections and initial device classification. https://www.iso.org/standard/74157.html.